Published in final edited form as:

J Opt. 2017 April ; 19(4): . doi:10.1088/2040-8986/19/4/043001.

Optical quantum memory based on electromagnetically induced transparency

Lijun Ma, **Oliver Slattery**, and **Xiao Tang**

Information Technology Laboratory, National Institute of Standards and Technology, 100 Bureau Dr, Gaithersburg, MD 20899, United States of America

Abstract

Electromagnetically induced transparency (EIT) is a promising approach to implement quantum memory in quantum communication and quantum computing applications. In this paper, following a brief overview of the main approaches to quantum memory, we provide details of the physical principle and theory of quantum memory based specifically on EIT. We discuss the key technologies for implementing quantum memory based on EIT and review important milestones, from the first experimental demonstration to current applications in quantum information systems.

Keywords

quantum memory; quantum communication; electromagnetic introduced transparency

1. Introduction

Quantum memory is used to temporally store quantum states and to retrieve them at a later time. When the quantum states are prepared and manipulated using photons, it is called optical quantum memory. Because current quantum systems are mainly based on photons, the term ‘quantum memory’ in this paper refers to optical quantum memory. As an important application example, quantum memory can synchronize operations in linear quantum computing [1–3] and quantum networks [4] by storing and releasing quantum bits at the desired times. By temporarily storing quantum states, quantum memory serves a critical role in teleportation-based quantum repeaters which enable long distance quantum communications beyond the loss limitation in optical fibers [5–7]. Furthermore, quantum memory can convert a heralded single-photon-pair source, such as from spontaneous parametric down conversion (SPDC) with an arbitrary emission time, into a deterministic one with a well-defined emission time [8]. In addition, quantum memory can be applied to precision quantum measurements based on the quantum interference of atomic ensembles and thereby improve the precision of magnetometry, atomic clocks and spectroscopy [9]. Because quantum memory plays such important roles in quantum information systems, the development of quantum memories is currently an active research area with a variety of approaches being proposed and experimentally demonstrated. So far, several comprehensive review articles on quantum memories have been published [10–15]. In this review, we will

Correspondence to: Xiao Tang.

focus on quantum memory based on electromagnetically induced transparency (EIT). Following this short introduction, we will present a brief overview of the current major quantum memory approaches in section 2. The theoretical background of EIT quantum memory is given in section 3 and the key techniques for EIT quantum memories are described in section 4. The progress in the development of applications for practical EIT quantum memories is reviewed in section 5. Finally, we conclude with an outlook of future research and applications for EIT quantum memories in section 6.

2. Overview of quantum memory approaches

The function of quantum memory is to convert a flying qubit into a stationary qubit, to store the quantum state for a period of time and to convert the stationary qubit back into a flying qubit at a required time. According to [14], current quantum memory approaches can be categorized into three schemes: (1) optically controlled memories; (2) engineered absorption; and (3) a hybrid scheme that combines these two schemes.

The optically controlled scheme uses a strong optical pulse to induce absorption of a photon into the storage medium. This type of memory typically uses a Λ (lambda) type three-energy-level structure (as shown in figures 1(a) and (b)). Two allowed transitions between the ground levels (|g⟩ and |s⟩) and the excited level (|e⟩) are for the signal and the control light. The transition between the two ground levels is forbidden for the long radiative lifetime of the storage state. The typical storage and retrieval process of this scheme is shown in figure 1(c). A strong control beam (also known as the coupling beam and whose wavelength is close to resonance between |s⟩ and |e⟩ levels) is applied to the storage medium and ensures that all atoms are in the ground level (|g⟩) before a single photon signal (also known as the probe light and whose wavelength is close to resonance between |g⟩ and |e⟩) enters into the medium. The control and signal beams must be in a two-photon resonance condition but each field can be detuned by an amount (Δ) from the excited level (|e⟩). After the signal pulse fully enters into the medium, the control beam reduces adiabatically to zero and the signal photons can be coherently mapped onto an atomic spin wave. The signal photons, with its quantum properties preserved, can be retrieved later by reapplying the control beam. In this scheme, the retrieval is on-demand—the signal can be retrieved immediately when the control beam is reapplied. However, the signal photon is emitted together with the strong control beam, resulting in a major noise issue. Currently, this scheme has two main approaches that are referred to as EIT and Raman quantum memory. EIT is an optical phenomenon in atoms that uses quantum interference to induce transparency into an otherwise resonant and opaque medium. EIT can be used for slow light, light storage and quantum memory applications. In EIT, the detuning, Δ, between the two-photon resonance and the excited level is small (within the linewidth of the excited level). Therefore, since the control and signal beams are on the resonant atomic transitions, the control beam does not need very high power but its usable bandwidth is limited to sub-MHz (for warm atomic vapor) and tens of MHz (for a laser trapped cold atom). The quantum memory based on EIT was first described by Fleischhauer and Lukin in 2000 [16] and has since been demonstrated experimentally with a variety of materials and approaches. EIT-based light applications are comprehensively reviewed in [12, 17, 18]. EIT quantum memory can be implemented using a warm atomic vapor [19–23], cold atoms [24–32], Bose–Einstein

condensate (BEC) [33–35] or rare-earth (RE) doped solid state materials [36]. Using EIT, long storage times of greater than 1 s for quantum memory [35] and greater than 1 min for optical memory have been demonstrated [37]. Currently, most EIT quantum memory schemes are based on rubidium (Rb) atoms or cesium (Cs) atoms, and the corresponding operating wavelengths are 780 nm and 795 nm for Rb or 852 nm and 895 nm for Cs. In comparison to EIT memory based on a warm atomic vapor, the cold atoms system can provide a much longer spin coherence time, resulting in a longer available storage time. On the other hand, atomic-vapor-based EIT only requires magnetic shielding and temperature control of the vapor cell, which is relatively inexpensive and scalable, while cold-atom-based EIT requires a magneto-optical trap (MOT) to prepare the atomic temperature to near zero kelvin. Raman quantum memory was first proposed in 2000 [38] and uses three energy levels in an atomic ensemble that is similar to EIT. The main difference is that the detuning (Δ) between the two-photon resonance and the excited level in Raman quantum memory is much larger and uses the off-resonant Raman interaction. Since, unlike EIT, the Raman-quantum-memory approach does not rely on a transparency effect, it has a larger operational bandwidth. Experiments have demonstrated over GHz storage bandwidth using Cs and Rb atoms and over THz with diamond and hydrogen molecules. Consequently, Raman quantum memory can store a temporally short pulse which necessarily comprises of a large range of frequencies, and is suitable for high-speed quantum memory [39]. In principle, the storage time of the Raman approach can match that of EIT memories, because the limitations to the coherence time are same for both approaches. Currently, using Raman quantum memory, storage times of up to 1.5 μs in warm gas vapor [40] and 500 ns in cold gas [41] have been experimentally demonstrated. Because it is implemented off resonance, Raman quantum memory requires a very strong control beam. The strong control beam likely causes spontaneous four-wave-mixing (SFWM), and results in a high number of noise photons that are in the same spatial, temporal and frequency mode as the retrieved signal photons [42]. The problem is particularly severe with implementations in warm atomic ensembles. Raman memory in cold atoms can eliminate large Doppler broadening and uses small off-resonant detuning and a weaker control field. Recently, Raman memory in cold atoms has been demonstrated with very low noise and has been used for non-classical light storage [41, 43]. Raman quantum memories are first realized experimentally by Walmsley's group in an atomic vapor [39, 44–46]. Several groups have since realized this type of quantum memory in cold atoms [41, 43], solid state [47, 48] and molecules [49]. The operating wavelengths for Raman quantum memory are dependent on the medium and include 852 nm (Cs vapor atom), 780 nm (cold Rb atom), 723 nm (diamond) [47, 48] and 600 nm (hydrogen molecules) [49].

The engineered absorption scheme is based on photon echo [50, 51] and is therefore also called the photon echo scheme. The quantum memory approaches based on this scheme include controlled reversible inhomogeneous broadening (CRIB) and atomic frequency combs (AFCs). In the CRIB protocol, first proposed in 2001 [52], atoms are excited by optical pump with a spectrally 'burned hole' to create a narrow absorption line and transfer other population into the auxiliary state and followed by an external electric or magnetic field to produce a controlled inhomogeneous broadening, which is reversed after a certain time to enable the re-emission of the stored light pulse (signal photons) by photon-echo. If

the direction of variation of the external electric or magnetic field is perpendicular to the propagation of the signal photons, it is called transverse CRIB. If the two directions are parallel, it is called longitudinal CRIB or, commonly, gradient echo memory (GEM). In the GEM protocol, the atomic detuning has a linearly varying spatial dependence, which, in principle, allows for a unity efficiency without additional techniques such as cavities or phase matching optical fields. The energy level structure together with the storage and retrieval process of CRIB are shown in figures 2(a) and (b). AFC, first proposed in 2009 [53], is another approach of photon-echo based quantum memories. In AFC, by using a spectrally comb-structured optical pump, the broad optical transition is shaped into a number of periodic and narrow absorption lines equally spaced in the frequency domain. The AFC plays a similar role to the inhomogeneous broadening in CRIB. After absorption of a quantum signal, whose bandwidth covers a few lines of the comb, the state of the light is transferred to collective atomic excitations, and atoms at different frequencies begin to dephase. Because of the periodic structure of the absorption line, a rephasing occurs after a time corresponding to the inverse of the frequency comb period (δ). When all the atoms return to an in-phase status, the light is re-emitted in the forward direction as a result of a collective interference between all the emitters. The energy level structure and the storage and retrieval process of AFC are shown in figures 2(c) and (d). Similar to CRIB, the AFC requires two energy levels for the storage and retrieval process and an auxiliary level for the absorption line structuring. Unlike CRIB however, AFC does not reverse the inhomogeneous broadening at the excited level, and the rephasing and re-emission of photons occurs after $1/\delta$. In other words, the storage time is pre-determined by the structure of the absorption comb lines. AFC is particularly suitable for a multimode storage situation because its multimode capacity is given by the number of the AFC comb lines and is independent of the medium optical density. In CRIB, the multimode capacity scales linearly with optical depth, whereas in EIT and Raman, it scales with the square root of the optical depth [54]. Currently, most CRIB and AFC quantum memory schemes use RE doped crystals, so the operating wavelengths correspond to the RE elements, such as 580 nm (europium), 606 nm (praseodymium), 793 nm (thulium), 880 nm (neodymium) and 1532 nm (erbium). Telecom-wavelength quantum memories have been demonstrated by this approach with erbium doped crystals [55] and erbium doped fiber [56]. Most CRIB and AFC quantum memories are implemented based on RE-ion doped solid state materials at cryogenic temperatures (<4 K). Some GEM approaches have also been demonstrated with a warm Rb atomic vapor [57–60]. The CRIB approach based on solid state has been reviewed in [61] in detail.

A hybrid scheme is a modified engineered absorption scheme which adopts a Λ type three-energy-level structure similar to the optically controlled scheme. The hybrid scheme holds all the advantages of the engineered absorption scheme, such as high mode capacity, low noise, realizable longer storage time and on-demand readout (although it has a delay after the second control pulse). Currently, the hybrid scheme has two successful approaches, Raman-GEM [59, 62] and Λ-AFC [63, 64]. Raman-GEM combines the Raman and GEM approaches and its energy structure and the storage and retrieval process are shown in figures 3(a) and (b). In Raman-GEM, there is no initial preparation of an absorption line and it uses the ground-state spin transition. A magnetic field gradient longitudinally broadens the transition lines and a control beam maps the signal state onto the broadened line coherently.

Reversing the polarity of the external magnetic field and applying another control pulse results in a re-phasing and re-emission of the signal photons. This approach has demonstrated a very high storage efficiency of 87% [59, 62]. The other hybrid scheme, Λ-AFC, uses three energy levels and an auxiliary level and its storage and retrieval process as shown in figures 3(c) and (d). Similar to the two-level AFC, the broadened transition is required to initiate an AFC by using an optical pump first. Λ-AFC then uses a strong control beam to map the coherence onto the spin wave of the atoms. When the signal needs to be read out, another control beam is applied and the process for the rephasing and re-emission of photons is resumed. The total storage time for all photons in Λ-AFC is the spin wave storage time (Ts) plus the fixed rephasing time($1/\delta$), which can be much longer than that of the two-level AFC. The spatial mode capacity for Λ-AFC is as high as for AFC. Another advantage for Λ-AFC is that the order of output photons is the same as the order of input photons since the storage time is the same for all photons.

Table 1 provides an overview of the current main quantum memory approaches. Although all of these approaches have been studied and demonstrated, EIT remains the most popular scheme for quantum memory and many groups have demonstrated quantum memory based on this approach [21, 25, 32, 33, 35, 37, 65–75]. In comparison to the other approaches, the EIT approach has a long storage time and is a relatively easy to implement and inexpensive solution. For example, EIT does not require the very high power control beam needed for Raman quantum memory, nor the liquid helium temperature required for CRIB or AFC. In addition, unlike approaches based on photon-echo, which have a time delay for the readout pulses to be generated due to the spin restoration in an inhomogeneously broadened medium, EIT can be read out at any time while the spin coherence survives. Although the operating wavelengths, bandwidth and mode capacity imposes some limits, corresponding technologies have been developed to make EIT quantum memory workable in quantum information systems.

3. Theoretical background of EIT optical quantum memory

EIT was first introduced by Harris and his co-workers at Stanford University in 1990 [79]. That work indicated that the optical response of an atomic medium is modified when laser beams lead to quantum interference between the excitation pathways which can eliminate absorption and refraction (linear susceptibility) at the resonant frequency of the atomic transition. Slow light, light storage and quantum memory have been implemented based on EIT. In this section, we will briefly review these theories using the formalisms and sign-systems used in [17] and [18].

EIT is the destructive interference of two light fields in a three-level atomic energy structure. There are three possible configurations for a three-level structure known as lambda (Λ), vee (V) and ladder, respectively, as shown in figure 4. We will focus on the lambda configuration, as it is the one most commonly used for implementing quantum memory.

In the lambda configuration, the transition between the two lower energy states, $|g\rangle$ and $|s\rangle$, is dipole-forbidden and atoms can stay in either of the two states for a long time. Both of the energy states have allowed transitions to an excited state, $|e\rangle$. In order to modify the

propagation through this atomic medium for an optical beam that couples the energy states |g⟩ and |e⟩, a strong optical beam can be applied that couples between the states |s⟩ and |e⟩. The two fields are resonant with the allowed transitions of the atoms, and the beams can be absorbed by the atoms if they enter the atomic medium alone. However, when the two beams are applied to the atomic medium simultaneously, they interfere destructively, and therefore none of the atoms are excited to the state |e⟩. As a consequence, the beams will not be absorbed.

The weak beam between |g⟩ and |e⟩ is called the 'signal' beam (it is also called the 'probe' beam) and the strong beam between |s⟩ and |e⟩ is called the 'control' beam (it is also called the 'coupling' beam). When the control beam is strong and its intensity is constant in time, the response of the atomic ensemble can be described in terms of the linear susceptibility spectrum $\chi^{(1)}(\omega)$, according to equation (1):

$$\chi^{(1)}(\omega)=g^2N\frac{\gamma_{\mathrm{gs}}+\mathrm{i}\omega}{(\gamma_{\mathrm{ge}}+\mathrm{i}\omega)(\gamma_{\mathrm{gs}}+\mathrm{i}\omega)+|\Omega|^2}, \quad (1)$$

where γ_{gs} and γ_{ge} are the decoherence rates of the $|g\rangle \rightarrow |s\rangle$ and $|g\rangle \rightarrow |e\rangle$ transitions respectively, ω is the Rabi frequency for the control field, N is the total number of atoms in the sample, g is the atom-field coupling constant, and ω is the frequency detuning of the resonance of the two optical fields (the signal and control fields). When $\omega = 0$, the two optical fields are resonant.

In an ideal EIT medium, the relaxation rate between the two lower energy states, |g⟩ and |s⟩, is very small, i.e. $\gamma_{\mathrm{gs}} \rightarrow 0$. Based on equation (1), the linear susceptibility spectrum of the EIT medium for a signal beam is shown in figure 5. The linear response of an atom to the light can be described by the linear susceptibility, $\chi^{(1)}$. The imaginary part of $\chi^{(1)}$ determines the dissipation of the field by the atomic gas, i.e. absorption, while the real part of $\chi^{(1)}$ determines the refractive index, n, of the EIT medium according to equation (2):

$$n=1+\frac{1}{2}\mathrm{Re}(\chi^{(1)}). \quad (2)$$

From figure 5(a), when $\omega = 0$, the imaginary part of $\chi^{(1)}$ goes to zero, which indicates no absorption at the atomic resonance. In other words, the medium is transparent due to the quantum interference. The transparency window is usually very narrow and determines the quantum memory operating bandwidth, as will be discussed later in this review. From figure 5(b), the real part of the susceptibility is zero at $\omega = 0$, and, according to equation (2), the refractive index equals 1. This implies that the phase velocity of the light is equal to that in a vacuum. However, in the narrow transparency window, the refractive index has a very steep variation with frequency, and this results in the group velocity being smaller than the speed of light in a vacuum in a phenomenon known as 'slow light'. From figures 5(a) and (b), the group velocity of signal light can be significantly reduced and, in the meantime, its

irreversible absorption can become very small at the two-field-resonance condition. These characteristics are desirable for quantum memory.

The phase velocity is the speed at which the zero-crossings of the carrier wave move; while the group velocity is the speed at which the peak of a wave packet moves. The two velocities are determined by equation (3):

$$\nu_{\mathrm{p}}=\frac{c}{n},\ \ \nu_{\mathrm{g}}=\frac{c}{n+\omega\frac{\partial n}{\partial\omega}}, \quad (3)$$

where ν_{p} and ν_{g} are the phase velocity and group velocity respectively, c is the speed of light in vacuum, n is the refractive index and ω is the frequency of light. If the refractive index does not change with frequency, the two velocities are the same. When the refractive index changes with respect to the frequency, then the group velocity will be smaller than phase velocity. In the case of very steep change, the group velocity will be greatly reduced.

According to equations (1)–(3), the group velocity of the signal beam is given by:

$$\nu_{\mathrm{g}}=\frac{c}{1+g^2N/|\Omega|^2}, \quad (4)$$

where N is the total number of atoms, as determined by the atomic density, in the sample, ω is the Rabi frequency of the control field and $|\Omega|^2$ is linearly proportional to control beam intensity. Therefore, the group velocity of the signal beam in the EIT medium is dependent on the atomic density and control beam intensity-increasing the atomic density or decreasing control beam intensity will reduce the group velocity of the signal beam.

EIT can significantly reduce the group velocity of a signal beam, and some experiments have demonstrated a signal beam velocity as slow as $c/10^6$ to $c/10^7$. EIT slow light can result in a great compression of the spatial profile of an optical pulse and can compress an optical pulse to a small spatial distance. In order to preserve the whole pulse, the velocity should be slow enough to compress the entire pulse into the medium. Therefore, the optical depth of the EIT medium should be significantly greater than one:

$$\alpha L=\frac{2g^2N}{\gamma_{\mathrm{ge}}c}L\gg 1, \quad (5)$$

where αL is the optical depth of the transition between $|\mathrm{g}\rangle \rightarrow |\mathrm{e}\rangle$ of the atomic medium. The spectral bandwidth of the transparency window of the EIT can be obtained by:

$$\Delta\omega_{\mathrm{EIT}}=\frac{2|\Omega|^2}{\gamma_{\mathrm{gs}}\sqrt{\alpha L}}. \quad (6)$$

The bandwidth of EIT transparency window is relevant to the decoherence rate, and in EIT quantum memory, the retrieval efficiency decay rate increases as the EIT bandwidth gets broader [80]. According to equation (6), a narrower bandwidth requires either reducing the control beam intensity or increasing the optical depth of the medium.

However, low control intensity or high optical depth would cause absorption during the propagation through the EIT medium. In the case of steady-state optical fields and assuming no absorption of the strong control beam, the signal beam intensity is given by:

$$|\varepsilon(z)|^2=|\varepsilon(0)|^2\ \exp\left(-\alpha L\frac{\gamma_{\mathrm{gs}}\gamma_{\mathrm{ge}}}{2|\Omega|^2}\right). \quad (7)$$

From equation (7), when the decoherence rate of the transition $|g\rangle \rightarrow |s\rangle$ (γ_{gs}) is not zero, dissipation (irreversible absorption) of the signal beam becomes larger as the optical depth (αL) becomes larger or as the control beam intensity ($|\Omega|^2$) becomes smaller. Therefore, in practice, a compromise of the two parameters is needed to achieve a narrow bandwidth with a modest absorption.

Although slow light with a static control beam can reduce the light velocity, it is not possible to completely stop a light pulse in a stationary EIT ensemble. To achieve the goal of storing and retrieving the light, the control beam must be changed. The intensity of the control beam influences the spectral bandwidth of the transparency window. Adiabatically changing the intensity of the control beam can impact the dynamics of the signal pulse with minimal loss. In particular, reducing the control beam intensity to zero can reduce the signal beam pulse velocity to zero, thereby storing the information carried by the signal pulse.

In [18], Lukin uses 'dark-state polaritons' to describe the propagation of the signal pulse through an EIT medium. A quantum field, $\Psi(z, t)$, is a superposition of a photonic component ($\mathcal{E}$ (z, t)) and an ensemble spin coherence component (S(z, t)) according to:

$$\Psi(\mathrm{z},\mathrm{t})=\cos(\theta)\mathscr{E}(\mathrm{z},\mathrm{t})-\sin(\theta)\mathrm{S}(\mathrm{z},\mathrm{t}), \quad (8)$$

where the mixing angle θ is given by:

$$\cos(\theta)=\frac{\Omega}{\sqrt{\Omega^2+g^2N}},\quad \sin(\theta)=\frac{g\sqrt{N}}{\sqrt{\Omega^2+g^2N}}. \quad (9)$$

After the signal beam pulse enters into the EIT medium and the control beam is reduced to zero ($\Omega = 0$), the dark-state polariton is comprised completely of an ensemble spin coherence. Consequently, the pulse is effectively stored in the EIT medium for a time up to the ensemble spin coherence lifetime ($T_2 = 1/\gamma_{gs}$). The pulse can be retrieved by switching the control beam back on, and the quantum states of the retrieved signal pulses are in principle identical to those of the input pulses.

4. Key technologies of EIT quantum memory

Although the theory of EIT quantum memory is similar to that of EIT light storage, quantum memory is significantly more technically challenging. Quantum memory must store and retrieve the fragile quantum states of single photons with high fidelity and therefore must achieve both high efficiency and low noise. In addition, the bandwidth of the photon source and the quantum memory must be compatible. We will discuss these technologies in this section.

4.1. Storage efficiency

Storage efficiency is defined as the probability of retrieving a single photon following storage in a quantum memory and is an important criterion for quantum information systems, such quantum repeaters.

Two issues are particularly significant for storage efficiency. Firstly, in order to avoid losses due to the cutoff of a pulse edge, it is desirable to have the entirety of the optical pulse within the EIT medium as described in the previous section. Therefore, the group velocity, v_g, should satisfy the condition $Tv_g \ll L$, where T is the input signal pulse duration and L is the length of the EIT medium. Secondly, it is desirable to have the entire spectral width of input pulse matched to and within the EIT atomic bandwidth, i.e. $\frac{1}{T} \ll \Delta\omega_{\mathrm{EIT}} \approx \sqrt{\alpha L}\nu_g/L$. To satisfy these two conditions simultaneously requires a very high optical depth $\alpha L \gg 1$. However, as mentioned previously, the high optical depth causes large absorption in the EIT medium. Consequently, for practical EIT quantum memory, the optical depth is typically moderately high ($\alpha L > 1$), and a compromise is made regarding the spatial, spectral and absorption factors.

A theoretical analysis by Gorshkov *et al* indicates that the optimal quantum storage efficiency fundamentally depends only on the optical depth αL [81], such that for any optical depth, there is a unique input pulse shape that provides the maximum storage efficiency. The analysis shows that under optimized conditions, the writing stage to the atomic storage is the time reverse of the retrieval stage from the atomic storage. Therefore, time-reversal symmetry can be used for the storage efficiency optimization, which uses successive time-reversal iterations to find the optimal signal pulse shape for a given control fields' temporal profile [81]. Novikova *et al* experimentally demonstrated a procedure for optimizing the storage efficiency in [82, 83]. The initial input signal pulse has a temporal Gaussian profile. Because the pulse shape is not optimal, the initial storage efficiency is approximately only 16%. The output signal is reversed and normalized and becomes the next iteration input pulse. After three iterations, a storage efficiency of 47% is achieved.

In 2012, Zhou *et al* experimentally demonstrated an EIT quantum memory scheme to optically store and retrieve heralded single-photon wave packets [32]. As shown in figure 6, narrow band single Stokes and anti-Stokes photon pairs are generated by SFWM in an ^{85}Rb cold atomic ensemble. The Stokes photons are detected as a heralded signal to trigger the waveform generator, and the anti-Stokes photons are shaped into an optimal waveform by the waveform generator and an electro-optical modulator. The heralded photons with the

controlled waveform are stored in an EIT quantum memory constructed of another ^{85}Rb cold atomic ensemble. The experiment demonstrated a storage efficiency of 49% with a temporal likeness of 96%.

4.2. Storage time and noise

Storage time and noise are also key criteria for quantum memory. Storage time is important for long-distance quantum communication and other applications as previously described. Noise will reduce the fidelity of any quantum measurement and quantum information system.

Storage time is mainly limited by the decoherence of the atom, which causes a loss of the stored spin wave state in the atomic ensemble [80]. Decoherence is mainly caused by the motion of the atoms (atoms may move out of the interaction region) and by perturbation of the atomic spin wave due to external effects such as magnetic field fluctuation and atomic collisions. Decoherence is worse in a warm atomic vapor than in trapped cold atoms due to the higher rate of collisions, resulting in shorter storage times and higher noise [80]. An anti-relaxation coating on the inner walls of an atomic vapor cell can reduce the decoherence caused by atom-wall collisions. Paraffin, which is formed from long-chain alkane molecules and can support approximately 10^4 atom-wall collisions before depolarizing the alkali-atom spins, is the most common coating material used. Recently, a new alkane-based coating is reported to support up to 10^6 polarization preserving bounces, and the coherence time can extend to as long as a minute [84, 85]. A noble gas can be added to the vapor cell as a buffer to reduce the atom movement, reducing collisions and increasing the storage time and read-out efficiency [86, 87]. However, although the collisions between atoms do not influence the stored ground-state hyperfine coherence, they may severely deteriorate the fidelity of the quantum memory when they happen during the write and read processes [88]. Therefore, a coated cell without buffer gas is currently considered to be the best way to implement EIT quantum memory based on warm atoms. Cold atoms have wall-free confinement and collisions happen many orders of magnitude fewer times than that in a warm atomic vapor cell.

In EIT quantum memory, a strong residual control beam comes out from the memory along with the readout single-photon-level signal. The strong residual control beam (in the order of mW) becomes the main source of noise in the system and must be removed (or greatly reduced by ≈ 120 dB) to satisfy the noise requirements of a single-photon level quantum system. Spatial, polarization and spectral filters can be used. Spatial filtering is achieved with an off-axis geometry in an atomic ensemble, and is widely used in EIT-quantum memory based on cold atoms. Using signal and control beam paths of just a few degree difference, the noise can be suppressed by 40 dB. The effective spatial filtering is limited by scattering from the surfaces around the atomic ensemble. Such spatial filters are not suitable for EIT quantum memory based on a warm atomic ensemble since it requires nearly collinear propagation of the signal and control beams to avoid large Doppler broadening [17]. Polarization filtering is commonly used for both cold and warm atomic ensemble-based EIT quantum memory systems, in which the signal and control beam are in perpendicular polarization states. A polarizer is then used to remove the control beam after

interaction with atomic ensembles. Birefringence of the optical elements used and imperfect extinction of the polarizers limit noise suppression of polarization filtering to approximately 60 dB extinction (using a Glan polarizer) of the control beam. Spectral filtering is also used to further remove residual control beam. However, traditional dispersive elements and interference filters are not suitable due to the small frequency difference of just a few GHz between the control and signal beams. Currently, atomic filters or Fabry–Perot (FP) etalons are used for spectral filtering in EIT quantum memory applications. Atomic filters are an efficient way to implement narrowband filtering near atomic transitions. There are two types of atomic filters used for EIT quantum memory including absorption atomic filters and Faraday atomic filters. An absorption atomic filter works like a narrowband notch filter that absorbs the light around the resonant wavelength of an allowed atomic transition while transmitting other wavelengths. As an example, the two isotopes of the Rb atom, ^{85}Rb and ^{87}Rb, have nearly degenerate transition lines, providing a convenient way to filter out the control beam. The nearly degenerate transition wavelength can be used for the control beam, and it is absorbed in the filtering isotope. Meanwhile, the filtering isotope does not have a transition at the signal wavelength, allowing the signal field to be transmitted [89, 90]. Many EIT quantum memory experiments have used ^{87}Rb as a memory medium and ^{85}Rb as an atomic filter [26, 86, 91]. Due to lack of suitable isotopes, Cs-based EIT quantum memory requires optically pumped atomic filters, in which the optical pump causes an allowed transition wavelength to become transparent in the filter [92]. A Faraday atomic filter works likes a narrow bandpass filter and can help to remove the control beam and other noise by rotating only the atomic transition wavelength polarizations by 90° as they pass passing through a vapor cell. A polarizer after the cell transmits the light at the atomic resonant wavelengths and blocks other wavelengths whose polarization has not been rotated. Similar to absorption atomic filters, Faraday atomic filters for Cs need an optical pump [93]. Figure 7(a) shows how a ^{85}Rb absorption atomic filter and a Faraday atomic filter are used for ^{87}Rb-based quantum memory [94]. Another type of spectral filter for EIT quantum memory applications is a FP etalon, typically providing only approximately 20 dB of control beam suppression. To further reduce noise, Hockel *et al* developed a multi-pass FP etalon (figure 7(b)) and achieved 46 dB of control beam suppression with 65% signal beam transmission. As shown in figure 7(b), two retroreflectors placed above and below the etalon direct the beams back through the etalon three times at different positions. Using a Glan polarizer and a multi-pass FP etalon, Hockel *et al* successfully demonstrated EIT quantum memory based on warm Cs atoms at the single photon level.

4.3. Photon source

The first experimental demonstration of single-photon-level EIT quantum memory used single photons that were generated from an atomic ensemble [86] because the wavelength and bandwidth of the source and memory are matched. The photon pair source, based on SFWM in a laser-cooled atomic system, can produce photons pairs with a linewidth of a few MHz and is suitable for EIT quantum memory based on cold atoms. This technology has been reviewed in [95]. However, the most common entangled photon sources for quantum information systems are based on SPDC with typically very broad linewidths (≈ THz). Such linewidths are orders of magnitude too broad for atomic ensemble based EIT, which require linewidths of tens of MHz for cold atoms and hundreds of KHz for warm atoms,

respectively. Early experiments of EIT quantum memory using single photons from an SPDC source used a series of extremely narrow filters [30, 31] or cavity narrowing and enhancement [26, 96–100] to achieve the linewidths required.

In addition to the narrow linewidth requirement, the operating wavelength of the SPDC photon source must match the atomic transition of the EIT ensemble, such as the D1 or D2 lines of the Rb or Cs atoms. Furthermore, dual-wavelength photon sources are favorable for long distance quantum systems with one wavelength suitable for the quantum memory and the other for low-loss transmission in optical fibers. Recently, our group developed a highly non-degenerate single photon-pair source, based on cavity enhanced SPDC, that is specifically tailored to interface with the D1 transition (894.6 nm) of the Cs atom for quantum memory and the low transmission loss near-infrared (1310 nm) telecommunication band for long-distance transmission [101].

The experimental setup, shown in figure 8, consists of three sections including the Cs atomic reference for locking of the cavity emission to the targeted atomic transition, the cavity-narrowed SPDC, and the filtering and detection of the SPDC generated photons from a small number of resonant modes. Initially, a laser is locked to the D1 line of the Cs atom and is used as a reference to which the cavity is locked and stabilized. The reference laser and SPDC pump are combined and directed through the cavity containing the SPDC crystal. The crystal is designed for SPDC of a 532 nm pump to a signal near 894.6 nm for Cs D1 transition line interaction and an idler beam centered at 1312.5 nm for long-distance transmission. The cavity is singly-resonant for the signal with both the pump and idler fields passing straight through. The cavity round-trip time is approximately 0.22 ns, giving a free spectral range of approximately 4.5 GHz. The measured cavity finesse is approximately 93, corresponding to a linewidth is approximately 48 MHz. This linewidth is confirmed by a second-order correlation measurement of signal and idler photons from the cavity, and is suitable for use in EIT quantum memory based on cold atoms. Following the cavity, the signal photons are reflected from a volume Bragg grating (VBG) (linewidth of ≈ 0.1 nm), which serves as a narrowband filter to reduce the number of modes. The idler photons are suitable for long distance fiber transmission.

4.4. Quantum interfaces for optical frequency conversion

Currently, EIT quantum memory schemes are mainly based on Cs or Rb, and the wavelengths are close to the resonant frequency of the D1 or D2 lines, e.g. 852 nm or 895 nm for Cs and 780 nm or 795 nm for Rb. For fiber-based quantum information systems, the telecommunication wavelength bands (1310 and 1550 nm) have the lowest transmission loss. Quantum interfaces convert the photon field between these wavelengths without changing their quantum state.

Quantum frequency conversion at the single-photon level has been studied since 1990 [102], when Kumar predicted that the quantum state of single photons can be preserved during the frequency conversion process. In 1992, Huang *et al* experimentally showed that the non-classical intensity correlation between twin beams was preserved after one beam was up-converted to another wavelength [103]. In 2001, Kim *et al* used up-conversion to implement a complete Bell state measurement (BSM) in a quantum teleportation scheme [104]. Since

then, several groups have successfully developed highly efficient frequency conversion schemes at single-photon levels by using periodically-poled bulk or waveguide non-linear optical devices [105–114]. A review paper has summarized these efforts [115].

Quantum interfaces include quantum frequency up-conversion and down-conversion. Frequency up-conversion typically refers to converting the frequency of input photons into a higher frequency (shorter wavelength) such as, for example, converting a telecom wavelength to an atomic transition wavelength. Conversely, frequency down-conversion refers to converting the frequency of input photons into a lower frequency (longer wavelength). Currently, most quantum interfaces use sum frequency generation (SFG) for up-conversion and difference frequency generation (DFG) for down-conversion through a process known as quasi-phase matching (QPM) in periodically-poled bulk or waveguide non-linear devices. QPM can enhance the non-linear conversion process and maintain positive energy flow from the input frequencies to the generated output frequencies, and QPM also enables the use of a higher non-linear coefficient than is possible with birefringent phase matching. The longer interaction distance leads to significantly higher conversion efficiencies. Internal single-photon conversion efficiencies of almost 100% have been demonstrated in QPM-periodically-poled lithium niobate (PPLN) waveguides.

As with all quantum systems, noise is a concern in quantum interfaces. The main sources of noise in the frequency conversion process are spontaneous Raman scattering (SRS) [107, 111, 116] and unwanted SPDC of the pump [117, 118]. Using a pump that has a longer wavelength than the signal to be converted can reduce the noise associated with SRS and SPDC. Additionally, a large spectral separation between the pump and the signal can reduce noise associated with the conversion of classical light in the pump tail. In addition, the noise spectrum is much broader than the input and converted output linewidths, so narrow spectral filtering can help further reduce the noise level. In [114], three different spectral filters were compared in the single photon up-conversion system, and it was shown that a VBG can achieve a low noise level, while maintaining a high single-photon total conversion efficiency.

In 2010, Rakher *et al* demonstrated an up-conversion quantum interface [119] as shown in figure 9. Input single photons near the telecom wavelength of 1310 nm were generated by the recombination of excitons in a single epitaxially-grown indium arsenide (InAs) quantum dot. With a 1550 nm pump light, the photons are up-converted by SFG in a PPLN waveguide to near 775 nm, close to the Rb D2 line with an internal conversion efficiency of ≈ 75%. Following conversion, the second-order intensity correlations are measured using a Hanbury-Brown and Twiss interferometer, and the results demonstrated that the up-converted photon maintains the quantum characteristics of the original photon with a measured $g^{(2)}(0) = 0.165 < 0.5$. Following that work, another experiment demonstrated that higher order temporal correlations (up to 4th order) of photons are preserved after frequency up-conversion in the same setup [120]. In 2014, Albrecht *et al* demonstrated a down-conversion quantum interface for Rb-based quantum memory to a telecom wavelength near 1552 nm [121]. As shown in figure 10, heralded single photons at 780 nm from a cold Rb atomic-ensemble-based quantum memory are converted to 1552 nm by DFG in a PPLN waveguide with a strong 1569 nm pump beam. The results show a significant amount of non-classical correlations are preserved between the heralding and converted photons.

In addition to SFG or DFG, four-wave-mixing (FWM) is also used in quantum interface applications. Radnaev *et al* used a FWM-based quantum interface to demonstrate quantum memory with a telecom photon in a cold, optically thick atomic ensemble of ^{87}Rb in an extended dark MOT [29]. With two pumps at different wavelengths, single photons at 795 nm from the Rb-based-quantum memory are down-converted to a telecom wavelength. The telecom wavelength photons are then up-converted in the same interface back to the near visible range for detection. The results demonstrate that the non-classical light behavior is preserved during the two frequency-conversion steps.

5. Research progress of EIT quantum memory

In this section, we review important progress milestones in the development of EIT quantum memory, from the first experimental demonstration of EIT and EIT quantum memory to its application in quantum information systems.

5.1. EIT, slow light and EIT optical memory of classical light

Soon after EIT was first proposed and termed by Harris *et al* [79], the first experimental demonstration was implemented by the same group in 1991 [122]. This experiment used neutral strontium (Sr) atoms with a lambda configuration. The signal and control beams are 337.1 nm and 570.3 nm respectively, corresponding to the 5s5p $^1P_1 \rightarrow$ 4d5d $^1D_2$ and 4d5p $^1D_2 \rightarrow$ 4d5d $^1D_2$ lines of the of Sr atom. The experimental results demonstrate that the optically thick medium can be rendered transparent for a quantum level signal beam through quantum interference of the signal and control beam. Since this early demonstration, many groups have implemented EIT in different media, such as Rb atomic vapor [123].

The first demonstration of slow light based on EIT (also by Harris' group in 1995 [124]) uses a pure lead (Pb) vapor in a 10 cm long cell with a density of 2×10^{14} atom cm^{-3}. A pulse group velocity as low as $c/165$ (where c is the speed of light in a vacuum) was observed. Further experiments have demonstrated group velocities of $c/3000$ in a Cs atomic vapor cell [125], $c/10^6$ in a Rb atomic vapor [126] and $c/(3 \times 10^6)$ in a Rb atomic vapor [127]. By 1999, Hau *et al* achieved a group velocity of just $c/(2 \times 10^7)$ or 15 m s^{-1} [128]. This experiment was performed with a gas of sodium (Na) atoms cooled to far below the temperature required for BEC. The medium consisted of a cloud of atomic Na containing several million atoms with a peak density of 5×10^{12} cm^{-3}. The near motionless atoms allow the control and signal beams to be propagated at right angles to each other. The high density atomic vapor with near zero atomic motion provides an ideal condition for EIT. Meanwhile, other EIT slow light experiments demonstrated pulse group velocities of $c/(4 \times 10^7)$ (8 m s^{-1} in a Rb vapor [129] and $c/(6 \times 10^6)$ (45 m s^{-1} in solid state (Pr doped Y_2SiO_5) [130].

Light storage based on EIT was first proposed in 2000 by Fleischhauer and Lukin [16]. The theoretical work predicts that EIT with a dynamic control beam allows the information in an input pulse of signal light to be linearly, coherently, and reversibly mapped with high efficiency into a collective atomic state and that it can be retrieved at a later time. The EIT optical storage and retrieval of classical light were experimentally demonstrated in Rb atomic vapor [131] and in Na atomic vapor [65] in 2001. In 2002, Lukin's group

demonstrated that the retrieved photons are phase coherent and that the storage process is a linear optical process [66]. These results were significant since they indicate that EIT memory is suitable for quantum processes, even though these experiments were demonstrated with classical and multiphoton pulses.

5.2. EIT quantum memory for non-classical light

The first effort to apply EIT quantum memory to store non-classical light used single photons generated from an atomic ensemble, taking advantage of the matching narrow bandwidth and wavelength of the atomic transitions. In 2005, two groups demonstrated EIT memory with a single-photon signal in a warm Rb atomic ensemble [86] and in a trapped cold Rb atomic ensemble [24]. In the experiment referenced in [86], Eisaman *et al* used two ^{87}Rb atomic ensembles as a source and memory respectively, as shown in figure 11. The source atomic ensemble first created a single spin excitation via Raman scattering combined with a 'write' pulse and a single-photon detection. Later the atomic excitation is converted to a single photon by a 'retrieve' pulse. The single photons are guided into the second atomic ensemble for EIT quantum memory. Following separation of the retrieved photon and control beam by a polarization beam-splitter (PBS) and an atomic filter based on a ^{85}Rb vapor cell, the second-order intensity correlation of the retrieved photons were measured using a Hanbury-Brown and Twiss interferometer. The results show that the non-classical features of these photons are preserved after considerable storage time in the EIT quantum memory.

In quantum information systems, most entangled photon sources are based on SPDC. As discussed earlier, SPDC photon sources have intrinsic linewidths that are too broad for EIT quantum memory applications. Early efforts to use SPDC sources for EIT quantum memory include Kuzuma's group [30, 31], which used direct filtering to achieve suitable linewidths. In their previous work [30], they reduced the linewidth of SPDC generated photons from approximately 10 THz into 23 GHz using a holographic grating (HG) and a polarization maintaining single-mode fiber (PMF). Since the linewidth was still larger than the EIT bandwidth, only a part of the SPDC spectrum was shown to be stored and retrieved. Later, they further reduced of the SPDC linewidth by way of additional filtering as described in [31]. As shown in figure 12, the photons generated by SPDC are filtered to achieve a linewidth of 9 MHz using a filtering cavity, an etalon and a combination of a HG and a polarization maintaining single-mode fiber (SMF). Using EIT quantum memory based on a laser trapped cold Rb atomic ensemble and with a bandwidth of approximately 12.6 MHz, a storage efficiency of approximately 14% was demonstrated. An anti-correlation measurement verified that the retrieved photons remained non-classical. However, extremely narrow bandpass filtering of SPDC discards most of the generated bandwidth leading to low photon pair rates. A more efficient approach to implement narrow-linewidth single photons from SPDC uses cavity enhancement, as discussed earlier, with many groups demonstrating cavity enhanced SPDC sources for quantum memory applications [96–100, 132].

5.3. EIT quantum memory for polarization qubits

Polarization encoded qubits are widely used in quantum information systems. And it is therefore desirable that quantum memory schemes can store and retrieve photons of arbitrary

polarization states. However, most EIT quantum memory schemes are designed to store single photons of a specific polarization to enable polarization filtering of the control field. To store and retrieve photons with arbitrary polarization states in EIT quantum memory, two spatially separated atomic ensembles can be used to store two orthogonal polarization states. The polarization state can be restored by combining the retrieved fields from the two quantum memory ensembles. For example, Cho *et al* implemented EIT quantum memory for storage of a polarization qubit [21] as shown in figure 13. The polarization modes of the original photon are spatially separated using a beam displacer, and stored in two spatially separated warm Rb atomic ensembles in a single vapor cell. After simultaneous retrieval, the two polarization states are recombined using another beam displacer. The polarization state of the retrieved field is analyzed and the results show that a process fidelity of better than 91% is achieved following a storage time of up to 16 μs. Several other experiments have demonstrated EIT based storage of polarization independent qubits with similar schemes [20, 25, 133–136].

In 2011, Zhang *et al* demonstrated EIT quantum memory of polarization entangled photons from a cavity-enhanced SPDC source [26]. The experimental set-up is shown in figure 14. A pair of photons is generated by applying a UV pump to a periodically poled potassium titanyl phosphate (PPKTP) crystal inside a cavity. One photon is coupled into a 60 m long SMF and guided to a polarization state analyzer. Another photon is directed through a 20 m long SMF to an EIT quantum memory scheme, consisting of two cold atomic ensembles for the vertical and horizontal polarization states respectively. Following retrieval, a FP cavity and an atomic filter are used to remove the control beam and other noise. Results of polarization measurements show an average polarization fidelity of 92% following a storage time of up to 200 ns.

5.4. EIT quantum memory for continuous variables

In many current quantum information systems, quantum information is encoded in the discrete nature of single photons, such as the polarization, to represent the two-basis state of the qubit. However, photons have other non-discrete degrees of freedom that can be used to encode information, such as its position and its momentum. In a continuous variable-based quantum information system, all quantum features of the qubit, such as superposition and entanglement are carried over to these continuous variables. So far, several quantum computing protocols and quantum communication protocols based on the continuous variables have been proposed [137–141]. The most commonly used variables are field quadratures, which are defined in terms of the electric field associated with an optical mode:

$$E = x\,\cos(\omega t) + p\,\sin(\omega t), \quad (10)$$

where ω is the optical carrier frequency and t is the time. The coefficients x and p represent the amplitude of the in-phase and out-of-phase field quadratures, which are associated with position and momentum [142], respectively. According to the Heisenberg uncertainty principle, position and momentum cannot be precisely measured simultaneously. An increase in the precision of one of these parameters increases the uncertainty of the other

parameter resulting in what is called a squeezed state. Squeezed states of light can be obtained through the optical frequency conversion process, and is useful for continuous variable-based quantum computing and communication.

EIT quantum memory has also been used to store and retrieve continuous-variable quantum optical fields, such as squeezed light. Kozuma's group, in particular, studied the propagation of squeezed light through an optically dense atomic ensemble under EIT conditions. Their early work demonstrated ultraslow propagation of squeezed vacuum field pulses through an EIT medium [143] and that the squeezing of a vacuum field was maintained during the propagation [144, 145]. In 2008, both Kozuma's and Lvovsky's groups demonstrated the storage and retrieval of squeezed vacuum pulses using laser-trapped cold Rb ensembles [146] and warm Rb ensembles [22], as shown in figures 15(a) and (b), respectively. In similar experimental setups, they used parametric down-conversion in PPKTP crystals to generate narrow-linewidth squeezed light (or vacuum optical fields) at the wavelength suitable for storage in an ^{87}Rb ensemble. The pump light is frequency doubled from a Ti:sapphire laser, and an optical homodyne detector is used to detect the quadrature amplitude of the squeezed vacuum retrieved from the EIT memory. The main difference between their two implementations is the EIT medium: one used laser-trapped cold ^{87}Rb ensembles and the other used warm ^{87}Rb ensembles in a vapor cell. The results of both experiments demonstrated that squeezed vacuum fields can be stored and retrieved by EIT quantum memory. Both experiments also observed degradation of the squeezing due to residual absorption by resonant atoms although improved experiments have since been implemented [147, 148].

5.5. EIT quantum memory for orbital angular momentum (OAM)

Since OAM was realized in a laser beam by Allen *et al* in 1992 [149], it has generated significant interest in many application areas, including optical communication systems [150]. Because of the inherent infinite dimensions of OAM space, information carried by photons encoded in OAM space can offer high channel capacity for quantum communications systems [151–153]. EIT quantum memories have been successfully demonstrated to store and retrieve photons with OAM. In 2013, Veissier *et al* reported EIT quantum memory based on a cold Cs atomic ensemble for weak laser light at the single-photon power level [154]. Later in 2013, Ding *et al* demonstrated EIT quantum memory based on cold Rb atomic ensembles for true non-classical OAM encoded single photons. Their experimental set-up and results are shown in figure 16. A cold ^{85}Rb atomic ensemble in figure 16(a) is used to generate non-classical correlated photon pairs based on SFWM using a double-lambda configuration. One photon in the pair is used as a trigger and the other is engineered to carry a variety of orbital angular momenta. The photon carrying the OAM is stored in EIT quantum memory based on another cold ^{85}Rb atomic ensemble as shown in figure 16(b). The experiment demonstrated the non-classical characteristics of photons, including the featured OAM structure, are preserved during the storage time. Traditionally, optical quantum memory is used to encode quantum information in the form of polarization, phase and so on. This experiment, together with others [155, 156], demonstrated that EIT quantum memories can store and retrieve single photons carrying

OAM, which enabled another type of qubit to be potentially used in future high capacity quantum communication systems.

5.6. Towards a quantum repeater

Quantum memory is an essential building block in the development of quantum repeaters. In 2001, Duan, Lukin, Cirac and Zoller proposed a scheme, known as the DLCZ protocol [158] to implement a quantum repeater. In the DLCZ protocol, quantum states can be transferred between atoms and photons, and then stored in atomic ensembles for long periods. The DLCZ protocol uses a built-in quantum memory that is based on off-resonant Raman scattering, and its retrieval process is the same as that in an EIT quantum memory [159]. The DLCZ protocol is based on atomic ensembles with a lambda configuration. The protocol begins by preparing all atoms in the ground state. As shown in figure 17(a), a weak write pulse illuminates an atomic ensemble and induces a Raman transition ($|g\rangle \rightarrow |e\rangle$) with a probability of $\ll 1$. Afterwards, it decays to the $|s\rangle$ ground state and emits a Raman scattered photon, also called a stokes photon. The stokes photon is collected in a certain mode as the signal field. Detection of the Stokes photon indicates an excitation of a single atom in the ensemble and that the ensemble has been prepared in the state $|s\rangle$. Later, a relatively strong read pulse is used to convert the stored atomic excitation into an idler field, as shown in figure 17(b). Due to collective enhancement, the second photon (an anti-Stokes photon) will be emitted in the direction determined by the phase matching condition. If two atomic ensembles are simultaneously illuminated by read pulses and the emission paths are combined at a beamsplitter, then when a single photon is detected, it is impossible to tell which of the two ensembles has emitted the photon, and the state of the two ensembles becomes an entangled superposition (figure 17(c)). This can be subsequently used as the basis of a quantum repeater. In 2007, Simon *et al* proposed a similar approach [160], in which photon-pair sources and quantum memories are used. Two simultaneously and coherently excited photon-pair sources at different locations generate a pair of photons at each location. EIT quantum memories are suitable candidates to be used as the external memories needed in this approach. The approach is shown in figure 17(b). One photon in the pairs is stored in the quantum memory and the other photon is sent out for photon interference and detection at a central station. Similar to the DLCZ protocol, a detection of a single photon heralds the entanglement of two quantum memories. The entanglement can be extended to longer distances by successive entanglement swapping to realize a quantum repeater. In comparison to the DLCZ protocol, this approach with a photon-pair source and a quantum memory provides more flexibility for wavelength selection and possesses higher efficiency due to the high mode quantum memory. Currently, this protocol is the most promising approach to implement a quantum repeater based on atomic ensembles. A detailed review on quantum repeater protocols based on atomic ensembles is given in [7].

Although the experimental realization of the full DLCZ protocol has not yet been achieved, many essential steps for a DLCZ-type quantum repeater have been experimentally demonstrated, including quantum teleportation with a built-in quantum memory. Quantum teleportation, initially proposed in 1993 [161], is a way to transfer the state of a quantum system from one location to another and has been experimentally demonstrated by many groups [162–170]. It is a key process for quantum repeaters and quantum computation

applications. Quantum teleportation can be combined with quantum memories to realize large-scale quantum communication and quantum computing networks. In 2008, Chen *et al* demonstrated quantum teleportation that included quantum memory. The experimental set-up is shown in figure 18. At Bob's side, anti-Stokes photons from two ^{87}Rb atomic ensembles are collected and combined, and sent to Alice's side through an optical fiber. At Alice's side, a photon with an unknown quantum state interferes with a photon arriving from Bob side on a beam-splitter to perform a BSM. The BSM results are then sent to Bob through a classical channel. Afterwards, the quantum states stored in the atomic ensemble at Bob side are converted into a photon state and the photon is emitted. By applying a corresponding polarization operation based on the BSM result, the quantum state of the newly emitted photons at Bob's side should be identical with the otherwise unknown quantum state of the photons originally at Alice's side. The teleported state in the experiment can be successfully read out after a storage time of up to 8 μs. Quantum teleportation with quantum memories represents an important step towards a quantum repeater.

6. Outlook

Over the last decade, many groups have successfully implemented a variety of EIT quantum memory schemes, and demonstrated their functionality with both classical and non-classical photon sources. Some schemes have been applied to quantum experiments. Although it is not easy to forecast future development, we believe the following aspects may represent a trend in EIT quantum memory research.

a. *Single atom or ion system*. Currently, most EIT quantum memory systems are based on atomic ensembles because it is very hard to couple a photon to a single atom in free space and an atomic ensemble can greatly increase the probability of interaction between a photon and an atom. However, quantum memory based on a single atom (charged or neutral) could provide a longer coherence time and can be implemented as quantum network nodes [171]. The quantum memory schemes based on single atoms usually need to trap the atom in a high-finesse cavity [172–174] or use a high numerical aperture confocal microscope [175–177], both of which are currently technically challenging. It is necessary to point out that, in practice, it is quite challenging to reach unity memory efficiency with large atom numbers, i.e. large optical depths. Therefore, cavity enhancement is also used in the development of memory systems based on atomic ensembles.

b. *Multimode capacity*. As we described in this review, in comparison with photon-echo-type approaches, EIT quantum memory lacks multimode capacity, which is one of main challenges towards building a workable quantum repeater with EIT based quantum memory. In the quantum repeater approach based on photon-pairs and quantum memory [160], the multimode capacity of quantum memory can significantly improve the entanglement rate. However, the temporal mode number is very limited in the EIT approach. In EIT quantum memory, all photons must be spatially compressed inside the memory medium before the control beam is turned off, so it requires an unfeasibly high optical depth to

implement temporal multimode. However, a spatially multiplexed scheme could increase the multimode capacity for EIT quantum memories. Such a scheme was proposed in 2007 [178] and experimentally demonstrated in 2009 [179].

c. *Scalability*. Currently, most proof-of-concept experiments are still plagued with high complexity and lack of scalability. Therefore, we expect one of the research trends in EIT quantum memory to focus on the implementation of compact and scalable functioning devices with atom-on-chip, solid state or fiber devices being good candidates. The technology of atom-on-chip began in 2001 [180, 181] and has been used for implementing BECs [182], optical lattices [183], atomic clocks [184] and magnetometers [185], all of which demonstrate the potential to implement chip-scale EIT quantum memory. Solid state is another promising solution to realize compact and scalable EIT quantum memories. EIT slow light and light storage experiments based on solid state media have been demonstrated since 2001 [130]. Pr^{3+} doped Y_2SiO_5 is considered a very promising candidate, due to its very long hyperfine population lifetimes, e.g. $T_1 \approx 100$ s [186, 187]. The EIT-based light storage experiments have demonstrated a storage time of tens of seconds [69]. More recently, an experiment demonstrated up to 40 s of light storage [37]. A DLCZ protocol using Pr^{3+} doped Y_2SiO_5 was also proposed in [188]. Additionally, fiber-based EIT quantum memory is a suitable choice for fiber-based quantum information systems, especially for quantum communications. Recently, an EIT optical memory scheme based on the interaction of cold cesium atoms with the evanescent field surrounding an optical nanofiber has been proposed and experimentally demonstrated [75, 189]. In addition, warm atoms in a hollow fiber [190] is a potential approach for EIT quantum memories. While EIT quantum memory based on these technologies face some technical challenges and have not yet been demonstrated, they have already shown the potential to dramatically reduce the device size and increase its scalability, which paves the way for the development of practical quantum information systems.

References

1. Knill E, Laflamme R, Milburn GJ. A scheme for efficient quantum computation with linear optics. Nature. 2001; 409:46–52. [PubMed: 11343107]
2. Kok P, Munro WJ, Nemoto K, Ralph TC, Dowling JP, Milburn GJ. Linear optical quantum computing with photonic qubits. Rev. Mod. Phys. 2007; 79:135.
3. Raussendorf R, Briegel HJ. A one-way quantum computer. Phys. Rev. Lett. 2001; 86:5188. [PubMed: 11384453]
4. Kimble HJ. The quantum internet. Nature. 2008; 453:1023–30. [PubMed: 18563153]
5. Gisin N, Thew R. Quantum communication. Nat. Photonics. 2007; 1:165–71.
6. Briegel H-J, Dür W, Cirac JI, Zoller P. Quantum repeaters: the role of imperfect local operations in quantum communication. Phys. Rev. Lett. 1998; 81:5932.
7. Sangouard N, Simon C, de Riedmatten H, Gisin N. Quantum repeaters based on atomic ensembles and linear optics. Rev. Mod. Phys. 2011; 83:33–80.
8. Eisaman M, Fan J, Migdall A, Polyakov S. Invited review article: single-photon sources and detectors. Rev. Sci. Instrum. 2011; 82:071101. [PubMed: 21806165]

9. Appel J, Windpassinger PJ, Oblak D, Hoff UB, Kjærgaard N, Polzik ES. Mesoscopic atomic entanglement for precision measurements beyond the standard quantum limit. Proc. Natl Acad. Sci. USA. 2009; 106:10960–5. [PubMed: 19541646]
10. Lvovsky AI, Sanders BC, Tittel W. Optical quantum memory. Nat. Photonics. 2009; 3:706–14.
11. Simon C, et al. Quantum memories. Eur. Phys. J. D. 2010; 58:1–22.
12. Hammerer K, Sørensen AS, Polzik ES. Quantum interface between light and atomic ensembles. Rev. Mod. Phys. 2010; 82:1041.
13. Bussières F, Sangouard N, Afzelius M, de Riedmatten H, Simon C, Tittel W. Prospective applications of optical quantum memories. J. Mod. Opt. 2013; 60:1519–37.
14. Heshami K, et al. Quantum memories: emerging applications and recent advances. J. Mod. Opt. 2016; 63:2005–28. [PubMed: 27695198]
15. Afzelius M, Gisin N, Riedmatten HD. Quantum memory for photons. Phys. Today. 2015; 68:6.
16. Fleischhauer M, Lukin M. Dark-state polaritons in electromagnetically induced transparency. Phys. Rev. Lett. 2000; 84:5094. [PubMed: 10990875]
17. Novikova I, Walsworth RL, Xiao Y. Electromagnetically induced transparency-based slow and stored light in warm atoms. Laser Photonics Rev. 2012; 6:333–53.
18. Lukin M. Colloquium: trapping and manipulating photon states in atomic ensembles. Rev. Mod. Phys. 2003; 75:457.
19. Julsgaard B, Sherson J, Cirac JI, Fiurasek J, Polzik ES. Experimental demonstration of quantum memory for light. Nature. 2004; 432:482–6. [PubMed: 15565148]
20. Cho Y-W, Kim Y-H. Storage and retrieval of thermal light in warm atomic vapor. Phys. Rev. A. 2010; 82:033830.
21. Cho YW, Kim YH. Atomic vapor quantum memory for a photonic polarization qubit. Opt Express. 2010; 18:25786–93. [PubMed: 21164923]
22. Appel J, Figueroa E, Korystov D, Lobino M, Lvovsky A. Quantum memory for squeezed light. Phys. Rev. Lett. 2008; 100:093602. [PubMed: 18352710]
23. Höckel D, Benson O. Electromagnetically induced transparency in cesium vapor with probe pulses on the single-photon level. Phys. Rev. Lett. 2010; 105:153605. [PubMed: 21230904]
24. Chaneliere T, Matsukevich D, Jenkins S, Lan S-Y, Kennedy T, Kuzmich A. Storage and retrieval of single photons transmitted between remote quantum memories. Nature. 2005; 438:833–6. [PubMed: 16341009]
25. Choi KS, Deng H, Laurat J, Kimble HJ. Mapping photonic entanglement into and out of a quantum memory. Nature. 2008; 452:67–U4. [PubMed: 18322529]
26. Zhang H, et al. Preparation and storage of frequency-uncorrelated entangled photons from cavity-enhanced spontaneous parametric downconversion. Nat. Photonics. 2011; 5:628–32.
27. Bao XH, et al. Efficient and long-lived quantum memory with cold atoms inside a ring cavity. Nat. Phys. 2012; 8:517–21.
28. Chen YA, et al. Memory-built-in quantum teleportation with photonic and atomic qubits. Nat. Phys. Feb.2008 4:103–7.
29. Radnaev AG, et al. A quantum memory with telecom-wavelength conversion. Nat. Phys. Nov.2010 6:894–9.
30. Akiba K, Kashiwagi K, Yonehara T, Kozuma M. Frequency-filtered storage of parametric fluorescence with electromagnetically induced transparency. Phys. Rev. A. 2007; 76:023812.
31. Akiba K, Kashiwagi K, Arikawa M, Kozuma M. Storage and retrieval of nonclassical photon pairs and conditional single photons generated by the parametric down-conversion process. New J. Phys. 2009; 11:013049.
32. Zhou S, et al. Optimal storage and retrieval of single-photon waveforms. Opt. Express. 2012; 20:24124–31. [PubMed: 23187175]
33. Riedl S, Lettner M, Vo C, Baur S, Rempe G, Dürr S. Bose–Einstein condensate as a quantum memory for a photonic polarization qubit. Phys. Rev. A. 2012; 85:022318.
34. Lettner M, et al. Remote entanglement between a single atom and a Bose–Einstein condensate. Phys. Rev. Lett. 2011; 106:210503. [PubMed: 21699281]

35. Zhang R, Garner SR, Hau LV. Creation of long-term coherent optical memory via controlled nonlinear interactions in Bose–Einstein condensates. Phys. Rev. Lett. 2009; 103:233602. [PubMed: 20366149]
36. Schraft D, Hain M, Lorenz N, Halfmann T. Stopped light at high storage efficiency in a Pr^{3+}: Y_2SiO_5 crystal. Phys. Rev. Lett. 2016; 116:073602. [PubMed: 26943534]
37. Heinze G, Hubrich C, Halfmann T. Stopped light and image storage by electromagnetically induced transparency up to the regime of one minute. Phys. Rev. Lett. 2013; 111:033601. [PubMed: 23909316]
38. Kozhekin A, Mølmer K, Polzik E. Quantum memory for light. Phys. Rev. A. 2000; 62:033809.
39. Reim KF, et al. Towards high-speed optical quantum memories. Nat. Photonics. 2010; 4:218–21.
40. England D, et al. High-fidelity polarization storage in a gigahertz bandwidth quantum memory. J. Phys. B. At. Mol. Opt. Phys. 2012; 45:124008.
41. Ding D-S, Zhang W, Zhou Z-Y, Shi S, Shi B-S, Guo G-C. Raman quantum memory of photonic polarized entanglement. Nat. Photonics. 2015; 9:332–8.
42. Sprague MR, et al. Broadband single-photon-level memory in a hollow-core photonic crystal fibre. Nat. Photonics. 2014; 8:287–91.
43. Ding D-S, et al. Quantum storage of orbital angular momentum entanglement in an atomic ensemble. Phys. Rev. Lett. 2015; 114:050502. [PubMed: 25699427]
44. Reim KF, Michelberger P, Lee KC, Nunn J, Langford NK, Walmsley IA. Single-photon-level quantum memory at room temperature. Phys. Rev. Lett. 2011; 107:053603. [PubMed: 21867069]
45. Reim KF, et al. Multipulse addressing of a raman quantum memory: configurable beam splitting and efficient readout. Phys. Rev. Lett. 2012; 108:263602. [PubMed: 23004977]
46. Nunn J, et al. Mapping broadband single-photon wave packets into an atomic memory. Phys. Rev. A. 2007; 75:011401.
47. England D, Bustard P, Nunn J, Lausten R, Sussman B. From photons to phonons and back: a THz optical memory in diamond. Phys. Rev. Lett. 2013; 111:243601. [PubMed: 24483658]
48. England DG, et al. Storage and retrieval of THz-bandwidth single photons using a room-temperature diamond quantum memory. Phys. Rev. Lett. 2015; 114:053602. [PubMed: 25699439]
49. Bustard PJ, Lausten R, England DG, Sussman BJ. Toward quantum processing in molecules: a THz-bandwidth coherent memory for light. Phys. Rev. Lett. 2013; 111:083901. [PubMed: 24010439]
50. Kurnit N, Abella I, Hartmann S. Observation of a photon echo. Phys. Rev. Lett. 1964; 13:567.
51. Abella I, Kurnit N, Hartmann S. Photon echoes. Phys. Rev. 1966; 141:391.
52. Moiseev S, Kröll S. Complete reconstruction of the quantum state of a single-photon wave packet absorbed by a Doppler-broadened transition. Phys. Rev. Lett. 2001; 87:173601–4. [PubMed: 11690273]
53. Afzelius M, Simon C, De Riedmatten H, Gisin N. Multimode quantum memory based on atomic frequency combs. Phys. Rev. A. 2009; 79:052329.
54. Nunn J, et al. Multimode memories in atomic ensembles. Phys. Rev. Lett. 2008; 101:260502. [PubMed: 19113761]
55. Lauritzen B, et al. Telecommunication-wavelength solid-state memory at the single photon level. Phys. Rev. Lett. 2010; 104:080502. [PubMed: 20366920]
56. Jin J, et al. Telecom-wavelength atomic quantum memory in optical fiber for heralded polarization qubits. Phys. Rev. Lett. 2015; 115:140501. [PubMed: 26551798]
57. Hétet G, Hosseini M, Sparkes B, Oblak D, Lam PK, Buchler BC. Photon echoes generated by reversing magnetic field gradients in a rubidium vapor. Opt. Lett. 2008; 33:2323–5. [PubMed: 18923610]
58. Hétet G, Longdell J, Sellars M, Lam PK, Buchler B. Multimodal properties and dynamics of gradient echo quantum memory. Phys. Rev. Lett. 2008; 101:203601. [PubMed: 19113339]
59. Hosseini M, Sparkes BM, Campbell G, Lam PK, Buchler BC. High efficiency coherent optical memory with warm rubidium vapour. Nat. Commun. 2011; 2:174. [PubMed: 21285952]
60. Hosseini M, Sparkes B, Campbell G, Lam PK, Buchler B. Storage and manipulation of light using a Raman gradient-echo process. J. Phys. B. At. Mol. Opt. Phys. 2012; 45:124004.

61. Tittel W, et al. Photon-echo quantum memory in solid state systems. Laser Photonics Rev. 2010; 4:244–67.
62. Cho Y-W, et al. Highly efficient optical quantum memory with long coherence time in cold atoms. Optica. 2016; 3:100–7.
63. Jobez P, Usmani I, Timoney N, Laplane C, Gisin N, Afzelius M. Cavity-enhanced storage in an optical spin-wave memory. New J. Phys. 2014; 16:083005.
64. Jobez P, et al. Coherent spin control at the quantum level in an ensemble-based optical memory. Phys. Rev. Lett. 2015; 114:230502. [PubMed: 26196785]
65. Liu C, Dutton Z, Behroozi CH, Hau LV. Observation of coherent optical information storage in an atomic medium using halted light pulses. Nature. 2001; 409:490–3. [PubMed: 11206540]
66. Mair A, Hager J, Phillips D, Walsworth R, Lukin M. Phase coherence and control of stored photonic information. Phys. Rev. A. 2002; 65:031802.
67. Dantan A, Pinard M. Quantum-state transfer between fields and atoms in electromagnetically induced transparency. Phys. Rev. A. 2004; 69:043810.
68. Dantan A, Bramati A, Pinard M. Atomic quantum memory: cavity versus single-pass schemes. Phys. Rev. A. 2005; 71:043801.
69. Longdell J, Fraval E, Sellars M, Manson N. Stopped light with storage times greater than one second using electromagnetically induced transparency in a solid. Phys. Rev. Lett. 2005; 95:063601. [PubMed: 16090952]
70. Hong T, et al. Realization of coherent optically dense media via buffer-gas cooling. Phys. Rev. A. 2009; 79:013806.
71. Schnorrberger U, et al. Electromagnetically induced transparency and light storage in an atomic Mott insulator. Phys. Rev. Lett. 2009; 103:033003. [PubMed: 19659274]
72. Chen Y-H, et al. Coherent optical memory with high storage efficiency and large fractional delay. Phys. Rev. Lett. 2013; 110:083601. [PubMed: 23473142]
73. Dudin Y, Li L, Kuzmich A. Light storage on the time scale of a minute. Phys. Rev. A. 2013; 87:031801.
74. Xu Z, et al. Long lifetime and high-fidelity quantum memory of photonic polarization qubit by lifting Zeeman degeneracy. Phys. Rev. Lett. 2013; 111:240503. [PubMed: 24483636]
75. Gouraud B, Maxein D, Nicolas A, Morin O, Laurat J. Demonstration of a memory for tightly guided light in an optical nanofiber. Phys. Rev. Lett. 2015; 114:180503. [PubMed: 26000992]
76. Sparkes B, et al. Gradient echo memory in an ultra-high optical depth cold atomic ensemble. New J. Phys. 2013; 15:085027.
77. Sabooni M, Li Q, Kroll S, Rippe L. Efficient quantum memory using a weakly absorbing sample. Phys. Rev. Lett. 2013; 110:133604. [PubMed: 23581321]
78. Maring N, et al. Storage of up-converted telecom photons in a doped crystal. New J. Phys. 2014; 16:113021.
79. Harris S, Field J, Imamoğlu A. Nonlinear optical processes using electromagnetically induced transparency. Phys. Rev. Lett. 1990; 64:1107. [PubMed: 10041301]
80. Figueroa E, Vewinger F, Appel J, Lvovsky A. Decoherence of electromagnetically induced transparency in atomic vapor. Opt. Lett. 2006; 31:2625–7. [PubMed: 16902640]
81. Gorshkov AV, André A, Fleischhauer M, Sørensen AS, Lukin MD. Universal approach to optimal photon storage in atomic media. Phys. Rev. Lett. 2007; 98:123601. [PubMed: 17501121]
82. Novikova I, Gorshkov AV, Phillips DF, Sørensen AS, Lukin MD, Walsworth RL. Optimal control of light pulse storage and retrieval. Phys. Rev. Lett. 2007; 98:243602. [PubMed: 17677964]
83. Novikova I, Gorshkov AV, Phillips DF, Xiao Y, Klein M, Walsworth RL. Optimization of slow and stored light in atomic vapor. Integrated Optoelectronic Devices 2007. 2007:64820M–64820M-11.
84. Balabas M, et al. High quality anti-relaxation coating material for alkali atom vapor cells. Opt. Express. 2010; 18:5825–30. [PubMed: 20389599]
85. Balabas M, Karaulanov T, Ledbetter M, Budker D. Polarized alkali-metal vapor with minute-long transverse spin-relaxation time. Phys. Rev. Lett. 2010; 105:070801. [PubMed: 20868027]
86. Eisaman M, André A, Massou F, Fleischhauer M, Zibrov A, Lukin M. Electromagnetically induced transparency with tunable single-photon pulses. Nature. 2005; 438:837–41. [PubMed: 16341010]

87. Andre A, Eisaman M, Walsworth R, Zibrov A, Lukin M. Quantum control of light using electromagnetically induced transparency. J. Phys. B. At. Mol. Opt. Phys. 2005; 38:S589.

88. Manz S, Fernholz T, Schmiedmayer J, Pan J-W. Collisional decoherence during writing and reading quantum states. Phys. Rev. A. 2007; 75:040101.

89. Heifetz A, Agarwal A, Cardoso GC, Gopal V, Kumar P, Shahriar M. Super efficient absorption filter for quantum memory using atomic ensembles in a vapor. Opt. Commun. 2004; 232:289–93.

90. Stack DT, Lee PJ, Quraishi Q. Simple and efficient absorption filter for single photons from a cold atom quantum memory. Opt. Express. 2015; 23:6822–32. [PubMed: 25836902]

91. Eisaman M, Childress L, André A, Massou F, Zibrov A, Lukin M. Shaping quantum pulses of light via coherent atomic memory. Phys. Rev. Lett. 2004; 93:233602. [PubMed: 15601158]

92. Kuzmich A, et al. Generation of nonclassical photon pairs for scalable quantum communication with atomic ensembles. Nature. 2003; 423:731–4. [PubMed: 12802329]

93. Hu Z, Zeng X. A laser pumped ultranarrow bandwidth optical filter. Appl. Phys. Lett. 1998; 73:2069–71.

94. Dąbrowski M, Chrapkiewicz R, Wasilewski W. Magnetically tuned, robust and efficient filtering system for spatially multimode quantum memory in warm atomic vapors. J. Mod. Opt. 2015; 63:1–10.

95. Du S, Wen J, Rubin MH. Narrowband biphoton generation near atomic resonance. JOSA B. 2008; 25:C98–108.

96. Bao X-H, et al. Generation of narrow-band polarization-entangled photon pairs for atomic quantum memories. Phys. Rev. Lett. 2008; 101:190501. [PubMed: 19113250]

97. Kuklewicz CE, Wong FN, Shapiro JH. Time-bin-modulated biphotons from cavity-enhanced down-conversion. Phys. Rev. Lett. 2006; 97:223601. [PubMed: 17155802]

98. Ou Z, Lu Y. Cavity enhanced spontaneous parametric down-conversion for the prolongation of correlation time between conjugate photons. Phys. Rev. Lett. 1999; 83:2556.

99. Scholz M, Koch L, Benson O. Statistics of narrowband single photons for quantum memories generated by ultrabright cavity-enhanced parametric down-conversion. Phys. Rev. Lett. 2009; 102:063603. [PubMed: 19257589]

100. Wolfgramm F, Xing X, Cere A, Predojević A, Steinberg A, Mitchell M. Bright filter-free source of indistinguishable photon pairs. Opt. Express. 2008; 16:18145–51. [PubMed: 18958092]

101. Slattery O, Ma L, Kuo P, Tang X. Narrow-linewidth source of greatly non-degenerate photon pairs for quantum repeaters from a short singly resonant cavity. Appl. Phys. B. 2015; 121:413–9.

102. Kumar P. Quantum frequency conversion. Opt. Lett. 1990; 15:1476–8. [PubMed: 19771127]

103. Huang J, Kumar P. Observation of quantum frequency conversion. Phys. Rev. Lett. 1992; 68:2153. [PubMed: 10045322]

104. Kim Y-H, Kulik SP, Shih Y. Quantum teleportation of a polarization state with a complete Bell state measurement. Phys. Rev. Lett. 2001; 86:1370. [PubMed: 11178086]

105. Vandevender AP, Kwiat PG. High efficiency single photon detection via frequency up-conversion. J. Mod. Opt. 2004; 51:1433–45.

106. Albota MA, Wong FN. Efficient single-photon counting at 1.55 μm by means of frequency upconversion. Opt. Lett. 2004; 29:1449–51. [PubMed: 15259709]

107. Langrock C, Diamanti E, Roussev RV, Yamamoto Y, Fejer MM, Takesue H. Highly efficient single-photon detection at communication wavelengths by use of upconversion in reverse-proton-exchanged periodically poled $LiNbO_3$ waveguides. Opt. Lett. 2005; 30:1725–7. [PubMed: 16075551]

108. Diamanti E, Takesue H, Honjo T, Inoue K, Yamamoto Y. Performance of various quantum-key-distribution systems using 1.55 μm up-conversion single-photon detectors. Phys. Rev. A. 2005; 72:052311.

109. Thew RT, et al. Low jitter up-conversion detectors for telecom wavelength GHz QKD. New J. Phys. 2006; 8:32.

110. Xu H, Ma L, Mink A, Hershman B, Tang X. 1310-nm quantum key distribution system with up-conversion pump wavelength at 1550 nm. Opt. Express. 2007; 15:7247–60. [PubMed: 19547047]

111. Pelc JS, et al. Long-wavelength-pumped upconversion single-photon detector at 1550 nm: performance and noise analysis. Opt. Express. 2011; 19:21445–56. [PubMed: 22108994]
112. Ma LJ, Slattery O, Tang X. Experimental study of high sensitivity infrared spectrometer with waveguide-based up-conversion detector. Opt. Express. Aug 3.2009 17:14395–404. [PubMed: 19654847]
113. Kuo PS, Slattery O, Kim YS, Pelc JS, Fejer MM, Tang X. Spectral response of an upconversion detector and spectrometer. Opt. Express. 2013; 21:22523–31. [PubMed: 24104141]
114. Kuo PS, Pelc JS, Slattery O, Kim YS, Fejer MM, Tang X. Reducing noise in single-photon-level frequency conversion. Opt. Lett. 2013; 38:1310–2. [PubMed: 23595468]
115. Ma LJ, Slattery O, Tang X. Single photon frequency up-conversion and its applications. Phys. Rep.—Rev. Sect. Phys. Lett. 2012; 521:69–94.
116. Zaske S, et al. Visible-to-telecom quantum frequency conversion of light from a single quantum emitter. Phys. Rev. Lett. 2012; 109:147404. [PubMed: 23083285]
117. Takesue H. Single-photon frequency down-conversion experiment. Phys. Rev. A. 2010; 82:013833.
118. Pelc JS, Langrock C, Zhang Q, Fejer MM. Influence of domain disorder on parametric noise in quasi-phase-matched quantum frequency converters. Opt. Lett. 2010; 35:2804–6. [PubMed: 20717463]
119. Rakher MT, Ma LJ, Slattery O, Tang XA, Srinivasan K. Quantum transduction of telecommunications-band single photons from a quantum dot by frequency upconversion. Nat. Photonics. Nov.2010 4:786–91.
120. Ma LJ, Rakher MT, Stevens MJ, Slattery O, Srinivasan K, Tang X. Temporal correlation of photons following frequency up-conversion. Opt. Express. 2011; 19:10501–10. [PubMed: 21643305]
121. Albrecht B, Farrera P, Fernandez-Gonzalvo X, Cristiani M, de Riedmatten H. A waveguide frequency converter connecting rubidium-based quantum memories to the telecom C-band. Nat. Commun. 2014; 5
122. Boller K-J, Imamoğlu A, Harris SE. Observation of electromagnetically induced transparency. Phys. Rev. Lett. 1991; 66:2593. [PubMed: 10043562]
123. Xiao M, Li Y-Q, Jin S-Z, Gea-Banacloche J. Measurement of dispersive properties of electromagnetically induced transparency in rubidium atoms. Phys. Rev. Lett. 1995; 74:666. [PubMed: 10058817]
124. Kasapi A, Jain M, Yin G, Harris SE. Electromagnetically induced transparency: propagation dynamics. Phys. Rev. Lett. 1995; 74:2447. [PubMed: 10057930]
125. Schmidt O, Wynands R, Hussein Z, Meschede D. Steep dispersion and group velocity below c 3000 in coherent population trapping. Phys. Rev. A. 1996; 53:R27. [PubMed: 9912934]
126. Lukin M, et al. Spectroscopy in dense coherent media: line narrowing and interference effects. Phys. Rev. Lett. 1997; 79:2959.
127. Kash MM, et al. Ultraslow group velocity and enhanced nonlinear optical effects in a coherently driven hot atomic gas. Phys. Rev. Lett. 1999; 82:5229.
128. Hau LV, Harris SE, Dutton Z, Behroozi CH. Light speed reduction to 17 metres per second in an ultracold atomic gas. Nature. 1999; 397:594–8.
129. Budker D, Kimball D, Rochester S, Yashchuk V. Nonlinear magneto-optics and reduced group velocity of light in atomic vapor with slow ground state relaxation. Phys. Rev. Lett. 1999; 83:1767.
130. Turukhin A, Sudarshanam V, Shahriar M, Musser J, Ham B, Hemmer P. Observation of ultraslow and stored light pulses in a solid. Phys. Rev. Lett. 2001; 88:023602. [PubMed: 11801011]
131. Phillips D, Fleischhauer A, Mair A, Walsworth R, Lukin MD. Storage of light in atomic vapor. Phys. Rev. Lett. 2001; 86:783. [PubMed: 11177939]
132. Nielsen BM, Neergaard-Nielsen J, Polzik ES. Time gating of heralded single photons for atomic memories. Opt. Lett. 2009; 34:3872–4. [PubMed: 20016642]
133. Tanji H, Ghosh S, Simon J, Bloom B, Vuletić V. Heralded single-magnon quantum memory for photon polarization states. Phys. Rev. Lett. 2009; 103:043601. [PubMed: 19659349]

134. Matsukevich D, Kuzmich A. Quantum state transfer between matter and light. Science. 2004; 306:663–6. [PubMed: 15499014]
135. Dudin Y, Radnaev A, Zhao R, Blumoff J, Kennedy T, Kuzmich A. Entanglement of light-shift compensated atomic spin waves with telecom light. Phys. Rev. Lett. 2010; 105:260502. [PubMed: 21231635]
136. Kupchak C, Mittiga T, Jordaan B, Namazi M, Nölleke C, Figueroa E. Room-temperature single-photon level memory for polarization states. Sci. Rep. 2015; 5
137. Braunstein SL, Van Loock P. Quantum information with continuous variables. Rev. Mod. Phys. 2005; 77:513.
138. Pirandola S, Mancini S, Lloyd S, Braunstein SL. Continuous-variable quantum cryptography using two-way quantum communication. Nat. Phys. 2008; 4:726–30.
139. Ralph TC. Continuous variable quantum cryptography. Phys. Rev. A. 1999; 61:010303.
140. Silberhorn C, Ralph TC, Lütkenhaus N, Leuchs G. Continuous variable quantum cryptography: beating the 3-dB loss limit. Phys. Rev. Lett. 2002; 89:167901. [PubMed: 12398756]
141. Zhang L, Silberhorn C, Walmsley IA. Secure quantum key distribution using continuous variables of single photons. Phys. Rev. Lett. 2008; 100:110504. [PubMed: 18517770]
142. Loudon, R. The Quantum Theory of Light. Oxford: Oxford University Press; 2000.
143. Akamatsu D, et al. Ultraslow propagation of squeezed vacuum pulses with electromagnetically induced transparency. Phys. Rev. Lett. 2007; 99:153602. [PubMed: 17995164]
144. Akamatsu D, Akiba K, Kozuma M. Electromagnetically induced transparency with squeezed vacuum. Phys. Rev. Lett. 2004; 92:203602. [PubMed: 15169353]
145. Arikawa M, et al. Observation of electromagnetically induced transparency for a squeezed vacuum with the time domain method. Opt. Express. 2007; 15:11849–54. [PubMed: 19547547]
146. Honda K, et al. Storage and retrieval of a squeezed vacuum. Phys. Rev. Lett. 2008; 100:093601. [PubMed: 18352709]
147. Arikawa M, et al. Quantum memory of a squeezed vacuum for arbitrary frequency sidebands. Phys. Rev. A. 2010; 81:021605.
148. Figueroa E, Lobino M, Korystov D, Appel J, Lvovsky A. Propagation of squeezed vacuum under electromagnetically induced transparency. New J. Phys. 2009; 11:013044.
149. Allen L, Beijersbergen MW, Spreeuw R, Woerdman J. Orbital angular momentum of light and the transformation of Laguerre–Gaussian laser modes. Phys. Rev. A. 1992; 45:8185. [PubMed: 9906912]
150. Franke-Arnold S, Allen L, Padgett M. Advances in optical angular momentum. Laser Photonics Rev. 2008; 2:299–313.
151. Leach J, et al. Quantum correlations in optical angle-orbital angular momentum variables. Science. 2010; 329:662–5. [PubMed: 20689014]
152. Dada AC, Leach J, Buller GS, Padgett MJ, Andersson E. Experimental high-dimensional two-photon entanglement and violations of generalized Bell inequalities. Nat. Phys. 2011; 7:677–80.
153. Fickler R, et al. Quantum entanglement of high angular momenta. Science. 2012; 338:640–3. [PubMed: 23118185]
154. Veissier L, et al. Reversible optical memory for twisted photons. Opt. Lett. 2013; 38:712–4. [PubMed: 23455274]
155. Nicolas A, Veissier L, Giner L, Giacobino E, Maxein D, Laurat J. A quantum memory for orbital angular momentum photonic qubits. Nat. Photonics. 2014; 8:234–8.
156. Parigi V, D'Ambrosio V, Arnold C, Marrucci L, Sciarrino F, Laurat J. Storage and retrieval of vector beams of light in a multiple-degree-of-freedom quantum memory. Nat. Commun. 2015; 6
157. Ding D-S, Zhou Z-Y, Shi B-S, Guo G-C. Single-photon-level quantum image memory based on cold atomic ensembles. Nat. Commun. 2013; 4
158. Duan LM, Cirac JI, Zoller P, Polzik ES. Quantum teleportation with atomic ensembles and coherent light. Quantum Commun. Comput. Meas. 2001; 3:351–7.
159. Eisaman, MD. PhD Thesis. Harvard University; 2006. Generation, storage, and retrieval of nonclassical states of light using atomic ensembles.

160. Simon C, de Riedmatten H, Afzelius M, Sangouard N, Zbinden H, Gisin N. Quantum repeaters with photon pair sources and multimode memories. Phys. Rev. Lett. 2007; 98:190503. [PubMed: 17677612]
161. Bennett CH, Brassard G, Crépeau C, Jozsa R, Peres A, Wootters WK. Teleporting an unknown quantum state via dual classical and Einstein–Podolsky–Rosen channels. Phys. Rev. Lett. 1993; 70:1895. [PubMed: 10053414]
162. Zhang Q, et al. Experimental quantum teleportation of a two-qubit composite system. Nat. Phys. 2006; 2:678–82.
163. Yonezawa H, Aoki T, Furusawa A. Demonstration of a quantum teleportation network for continuous variables. Nature. 2004; 431:430–3. [PubMed: 15386006]
164. Yin J, et al. Quantum teleportation and entanglement distribution over 100 kilometres free-space channels. Nature. 2012; 488:185–8. [PubMed: 22874963]
165. Sherson JF, et al. Quantum teleportation between light and matter. Nature. 2006; 443:557–60. [PubMed: 17024089]
166. Olmschenk S, Matsukevich DN, Maunz P, Hayes D, Duan LM, Monroe C. Quantum teleportation between distant matter qubits. Science. 2009; 323:486–9. [PubMed: 19164744]
167. Nilsson J, et al. Quantum teleportation using a light-emitting diode. Nat. Photonics. Apr.2013 7:311–5.
168. Ma XS, et al. Quantum teleportation over 143 kilometres using active feed-forward. Nature. 2012; 489:269–73. [PubMed: 22951967]
169. Bouwmeester D, Pan JW, Mattle K, Eibl M, Weinfurter H, Zeilinger A. Experimental quantum teleportation. Nature. 1997; 390:575–9.
170. Jin XM, et al. Experimental free-space quantum teleportation. Nat. Photonics. 2010; 4:376–81.
171. Duan L-M, Monroe C. Colloquium: quantum networks with trapped ions. Rev. Mod. Phys. 2010; 82:1209.
172. Specht HP, et al. A single-atom quantum memory. Nature. 2011; 473:190–3. [PubMed: 21532588]
173. Boozer AD, Boca A, Miller R, Northup TE, Kimble HJ. Reversible state transfer between light and a single trapped atom. Phys. Rev. Lett. 2007; 98:193601. [PubMed: 17677620]
174. Bochmann J, et al. Fast excitation and photon emission of a single-atom-cavity system. Phys. Rev. Lett. 2008; 101:223601. [PubMed: 19113483]
175. Tey MK, et al. Strong interaction between light and a single trapped atom without the need for a cavity. Nat. Phys. 2008; 4:924–7.
176. Tey MK, et al. Interfacing light and single atoms with a lens. New J. Phys. 2009; 11:043011.
177. Sondermann M, Maiwald R, Konermann H, Lindlein N, Peschel U, Leuchs G. Design of a mode converter for efficient light-atom coupling in free space. Appl. Phys. B. 2007; 89:489–92.
178. Collins O, Jenkins S, Kuzmich A, Kennedy T. Multiplexed memory-insensitive quantum repeaters. Phys. Rev. Lett. 2007; 98:060502. [PubMed: 17358924]
179. Lan S-Y, Radnaev A, Collins O, Matsukevich D, Kennedy T, Kuzmich A. A multiplexed quantum memory. Opt. Express. 2009; 17:13639–45. [PubMed: 19654771]
180. Hänsel W, Hommelhoff P, Hänsch T, Reichel J. Bose–Einstein condensation on a microelectronic chip. Nature. 2001; 413:498–501. [PubMed: 11586353]
181. Ott H, Fortagh J, Schlotterbeck G, Grossmann A, Zimmermann C. Bose–Einstein condensation in a surface microtrap. Phys. Rev. Lett. 2001; 87:230401. [PubMed: 11736434]
182. Du S, et al. Atom-chip Bose–Einstein condensation in a portable vacuum cell. Phys. Rev. A. 2004; 70:053606.
183. Straatsma CJ, Ivory MK, Duggan J, Ramirez-Serrano J, Anderson DZ, Salim EA. On-chip optical lattice for cold atom experiments. Opt. Lett. 2015; 40:3368–71. [PubMed: 26176471]
184. Vanier J. Atomic clocks based on coherent population trapping: a review. Appl. Phys. B. 2005; 81:421–42.
185. Shah V, Knappe S, Schwindt PD, Kitching J. Subpicotesla atomic magnetometry with a microfabricated vapour cell. Nat. Photonics. 2007; 1:649–52.

186. Holliday K, Croci M, Vauthey E, Wild UP. Spectral hole burning and holography in an Y_2SiO_5: Pr^{3+} crystal. Phys. Rev. B. 1993; 47:14741.

187. Nilsson M, Rippe L, Kröll S, Klieber R, Suter D. Hole-burning techniques for isolation and study of individual hyperfine transitions in inhomogeneously broadened solids demonstrated in Pr^{3+}: Y_2SiO_5. Phys. Rev. B. 2004; 70:214116.

188. Eisaman MD, Polyakov S, Hohensee M, Fan J, Hemmer P, Migdall A. Optimizing the storage and retrieval efficiency of a solid-state quantum memory through tailored state preparation. Optics East 2007. 2007:67800K–7800K.

189. Patnaik AK, Liang J, Hakuta K. Slow light propagation in a thin optical fiber via electromagnetically induced transparency. Phys. Rev. A. 2002; 66:063808.

190. Benabid F, Antonopoulos G, Knight J, Russell PSJ. Stokes amplification regimes in quasi-CW pumped hydrogen-filled hollow-core photonic crystal fiber. Phys. Rev. Lett. 2005; 95:213903. [PubMed: 16384142]

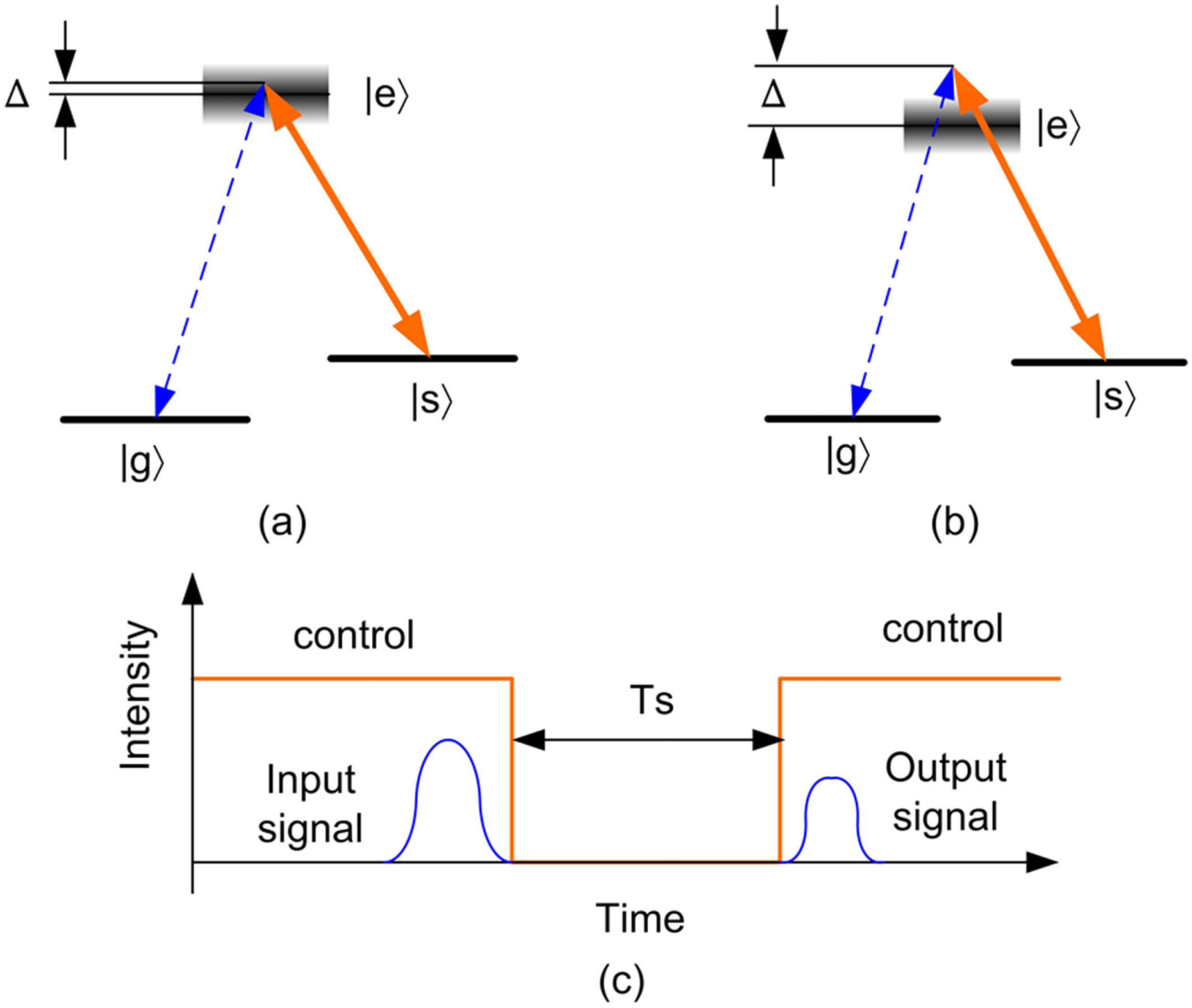

Figure 1.

Optically controlled scheme (a) energy level structure of EIT approach, (b) energy level structure of Raman approach, (c) storage and retrieval process of EIT and Raman. Ts: spin wave storage time.

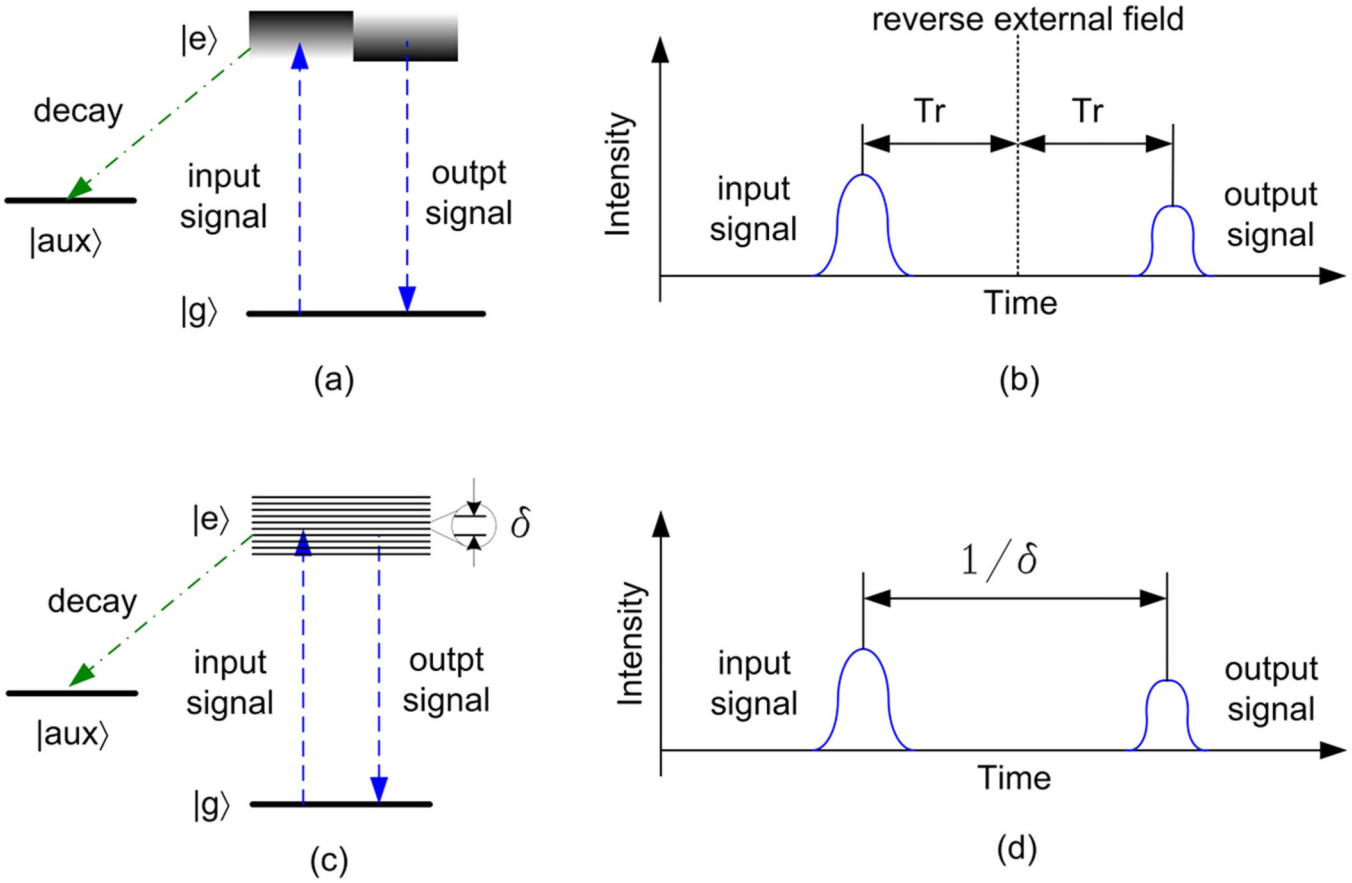

Figure 2.

Engineered absorption scheme (a) energy level structure of CRIB (b) storage and retrieval process of CRIB, (c) energy level structure of AFC, (d) storage and retrieval process of AFC. Tr: the time between signal input and the external field reverse.

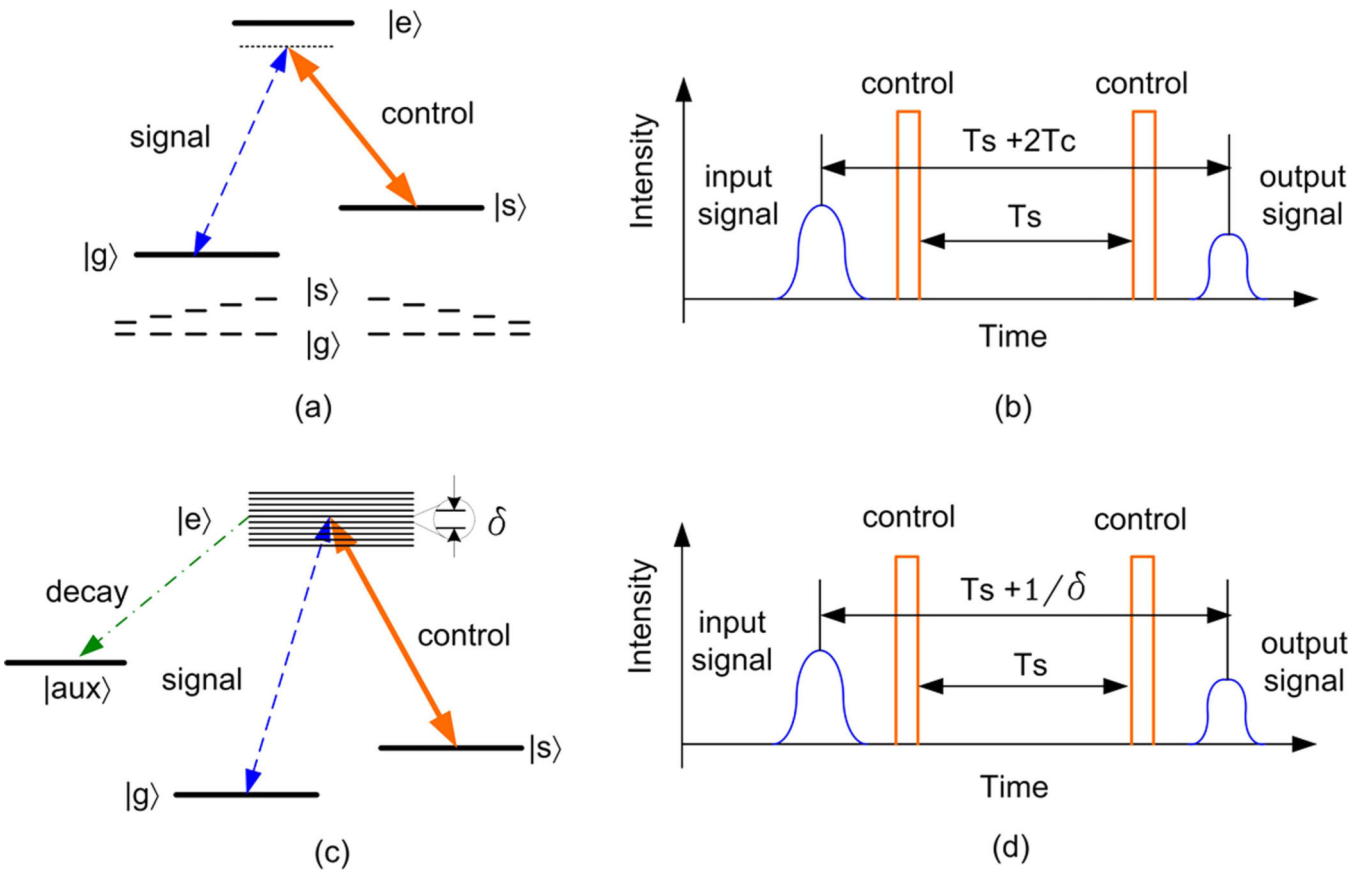

Figure 3.

Hybrid scheme (a) energy level structure of Raman-GEM, (b) storage and retrieval process of Raman-GEM. (c) Energy level structure of Λ-AFC, (d) storage and retrieval process of Λ-AFC. Ts: spin wave storage time. Tc: the time between signal pulse and control pulse.

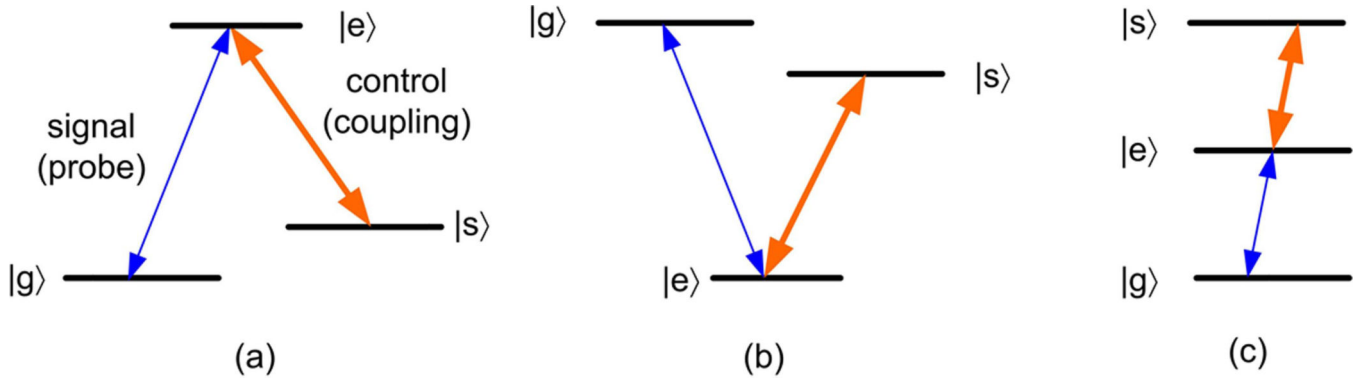

Figure 4.
Three possible configuration of EIT, (a) lambda, (b) vee and (c) ladder.

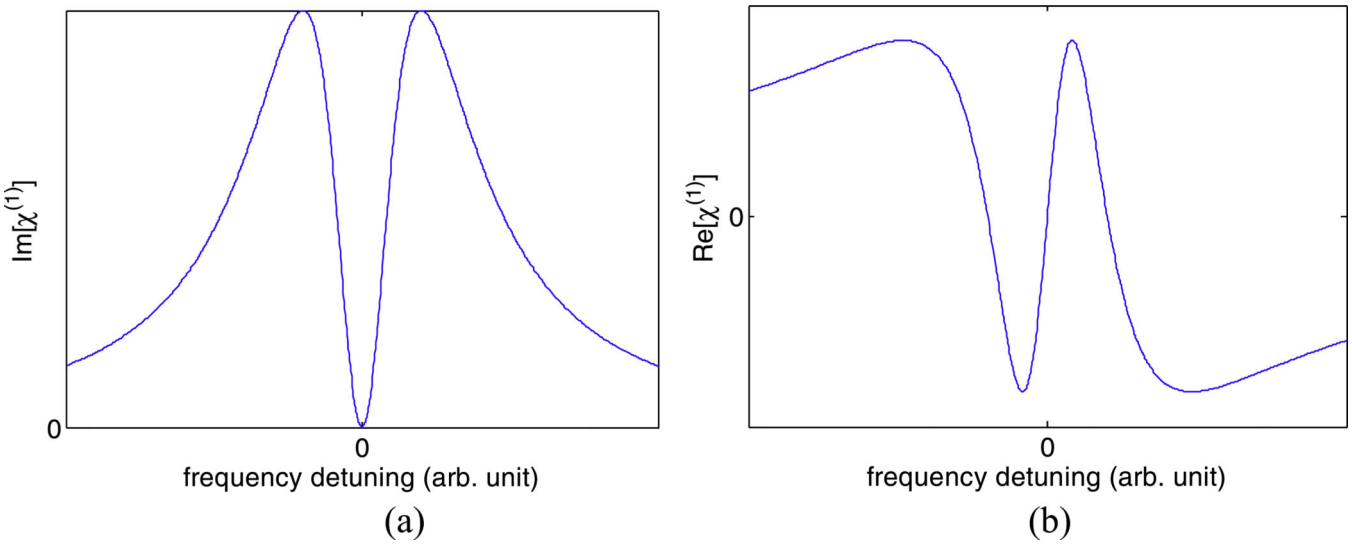

Figure 5.

Susceptibility as a function of the frequency detuning in an EIT medium: (a) imaginary part of $\chi^{(1)}$ characterizing absorption, (b) real part of $\chi^{(1)}$ determining the refractive properties of the medium.

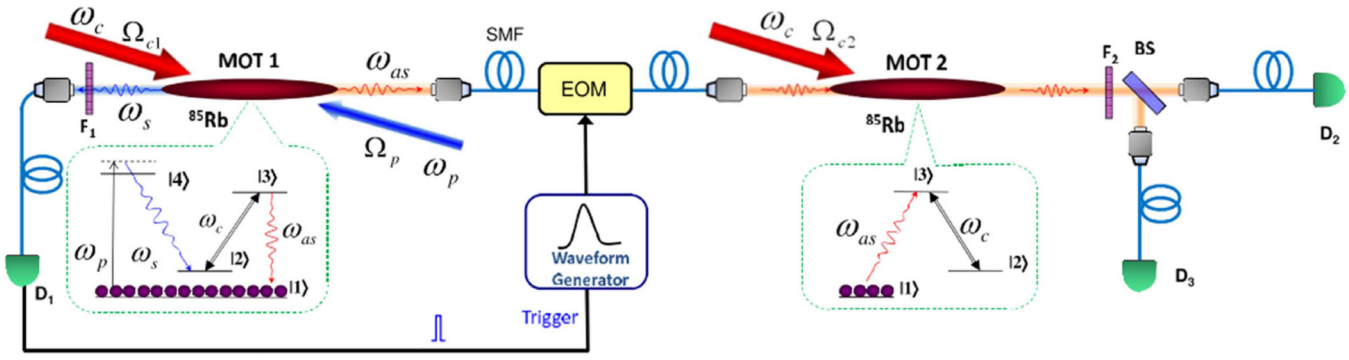

Figure 6.

Optimal storage and retrieval of single-photon waveforms. MOT: magneto-optical trapping; EOM: electro optical modulator. Reprinted figure with permission from [32], copyright 2016 by The Optical Society.

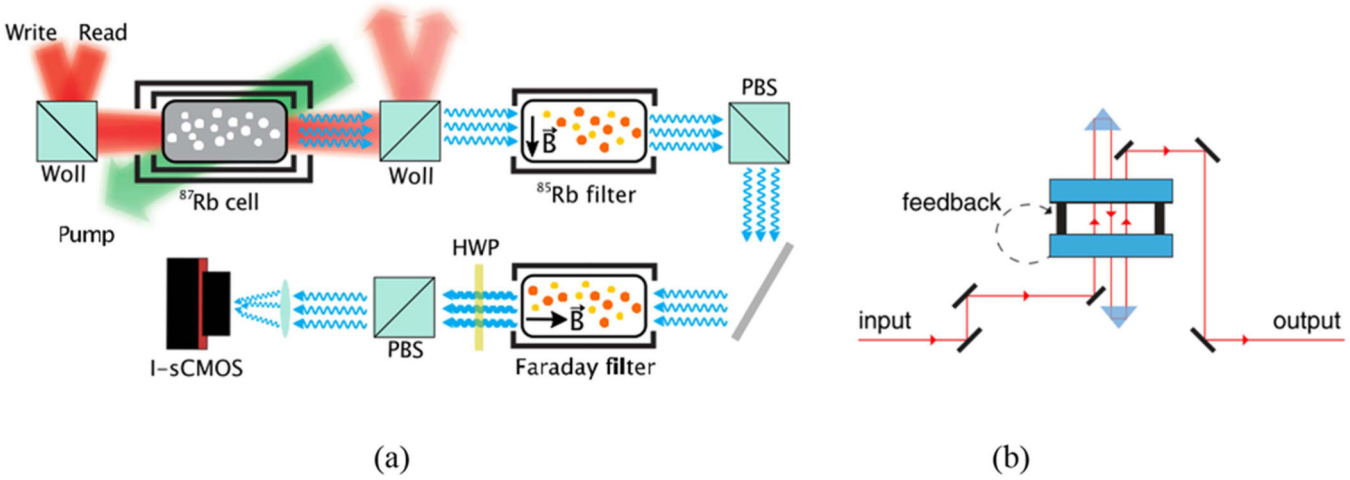

Figure 7.

Spectral filters used for EIT quantum memory. (a) Absorption atomic filters and Faraday atomic filter. (Woll: Wollaston polarizers, PBS: polarizing beam splitter, HWP: half-wave plate, I-sCMOS: intensified sCMOS camera). Reproduced with permission from [94], copyright 2015 Taylor & Francis; (b) Fabry–Perot etalon. Reprinted figure with permission from [23], copyright 2016 by the American Physical Society.

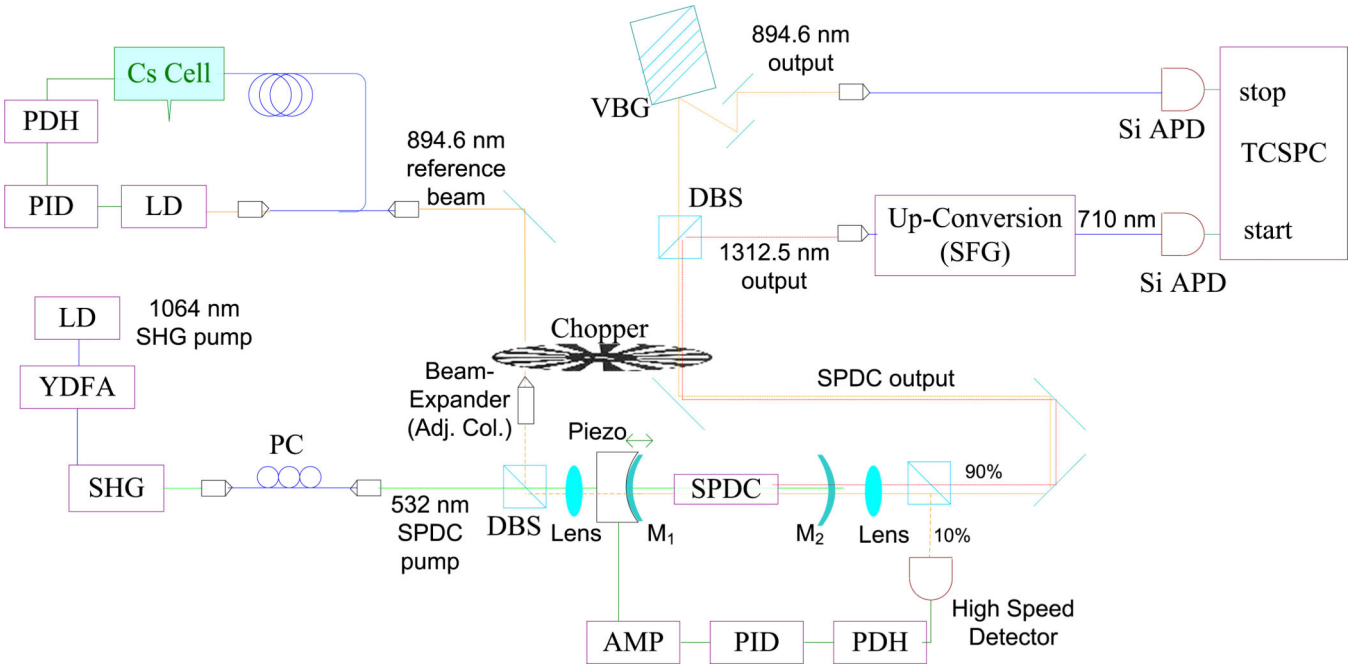

Figure 8.

Narrow linewidth non-generate SPDC photon source. LD: laser diode; YDFA: ytterbium doped fiber amplifier. PDH: Pound–Drever–Hall module; PID: proportional-integral-differential module; AMP: electrical amplifier; beam-expander (Adj. Col.): adjustable collimation beam-expander; SHG: second-harmonic-generation; PC: polarization controller; DBS: dichroic beam splitter/combiner; M1: input mirror; M2 output mirror; SPDC: spontaneous-parametric-down-conversion; VBG: volume Bragg grating; SFG: sum-frequency-generation; Si-APD: silicon avalanche photodiode; TCSPC: time correlated single photon counter. Reproduced with permission from [101]. Copyright 2015 Springer.

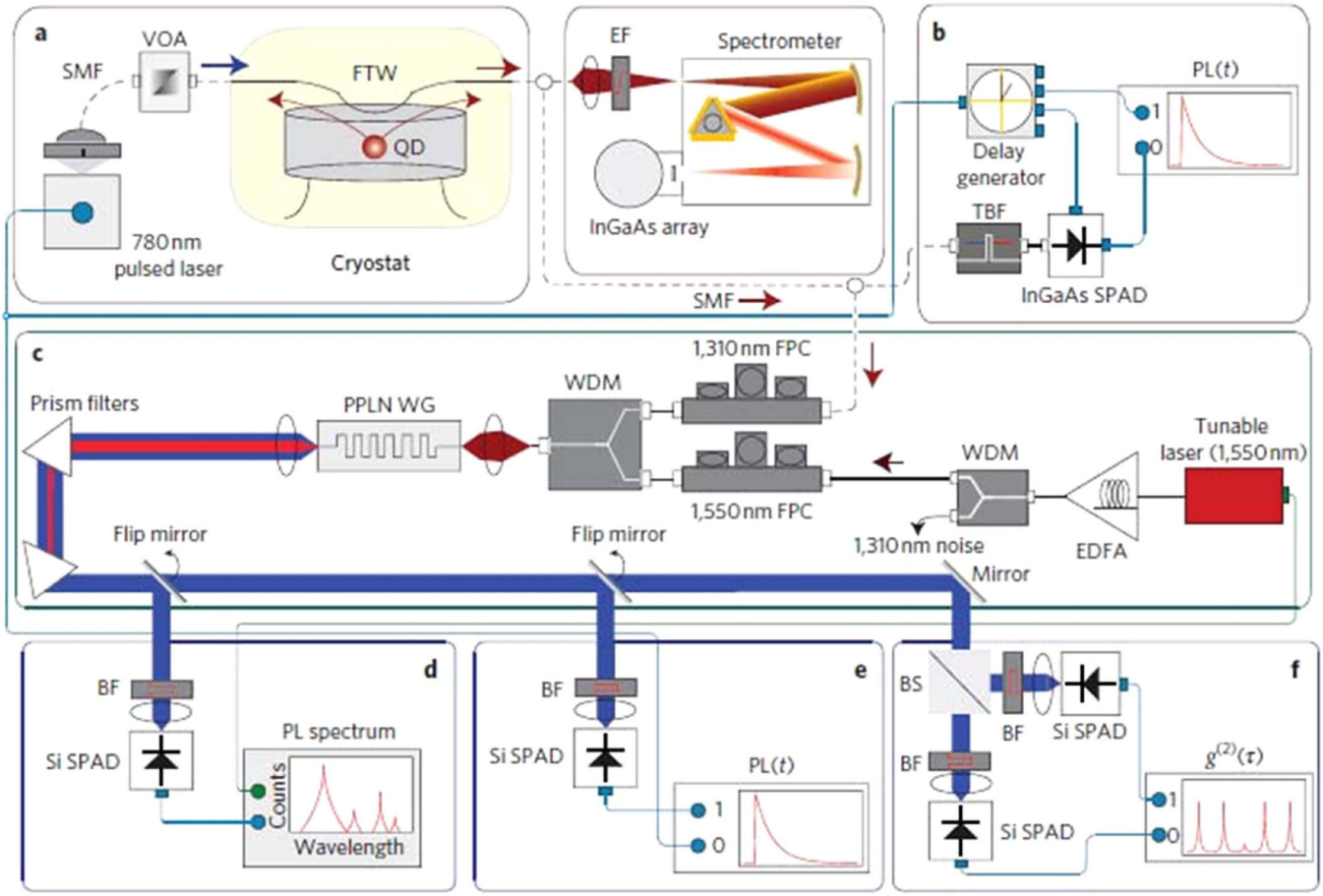

Figure 9.

Up-conversion quantum interface based on a PPLN waveguide for use with single photons from quantum dot. (PL, photoluminescence; Si SPAD, silicon single photon avalanche photodiode; FTW, fiber taper waveguide; SMF, single-mode fiber; VOA, variable optical attenuator; FPC, fiber polarization controller; WDM, wavelength division multiplexer; EDFA, erbium-doped fiber amplifier; TBF, tunable bandpass filter; EF, edge-pass filter; BF, bandpass filter; BS, non-polarizing beamsplitter; PPLN WG, periodically poled $LiNbO_3$ waveguide). Reprinted by permission from Macmillan Publishers Ltd: Nature Photonics [119], copyright (2010).

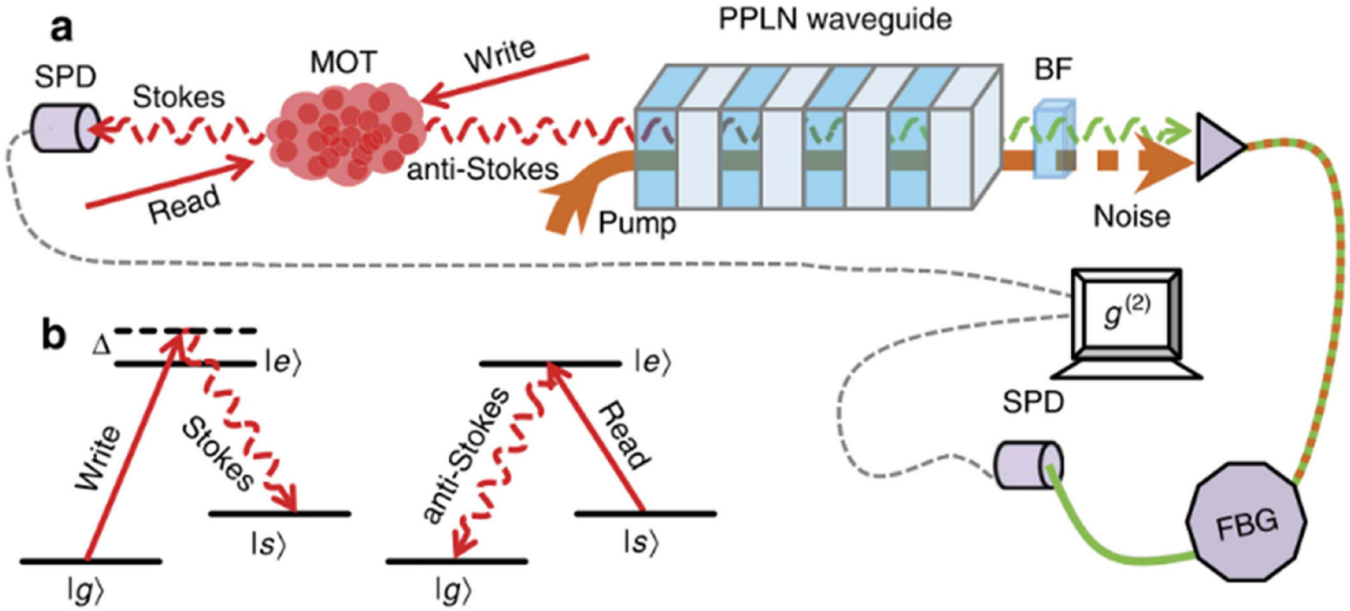

Figure 10.

Down-conversion quantum interface based on a PPLN waveguide for use with quantum memory. BF: bandpass filter; SPD: single photon detector; MOT: magneto-optical trap. Reprinted by permission from Macmillan Publishers Ltd: Nature Communications [121], copyright (2016).

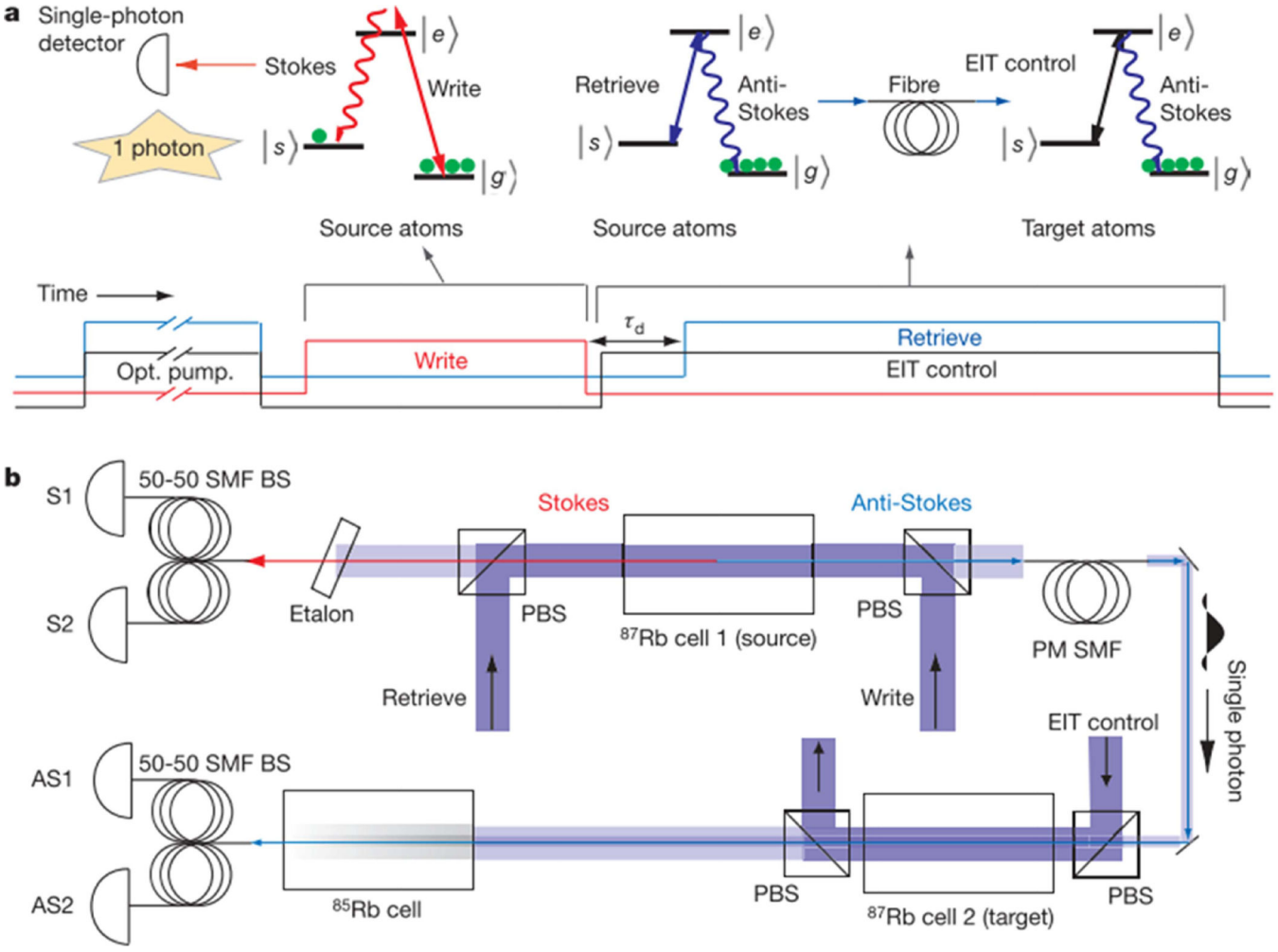

Figure 11.

Experiment of EIT quantum memory with single photon. PBS: polarizing beam splitter; PM SMF: polarization maintaining single mode fiber. SMF BS: single mode fiber beam splitter. Reprinted by permission from Macmillan Publishers Ltd: Nature Communications [86], copyright (2016).

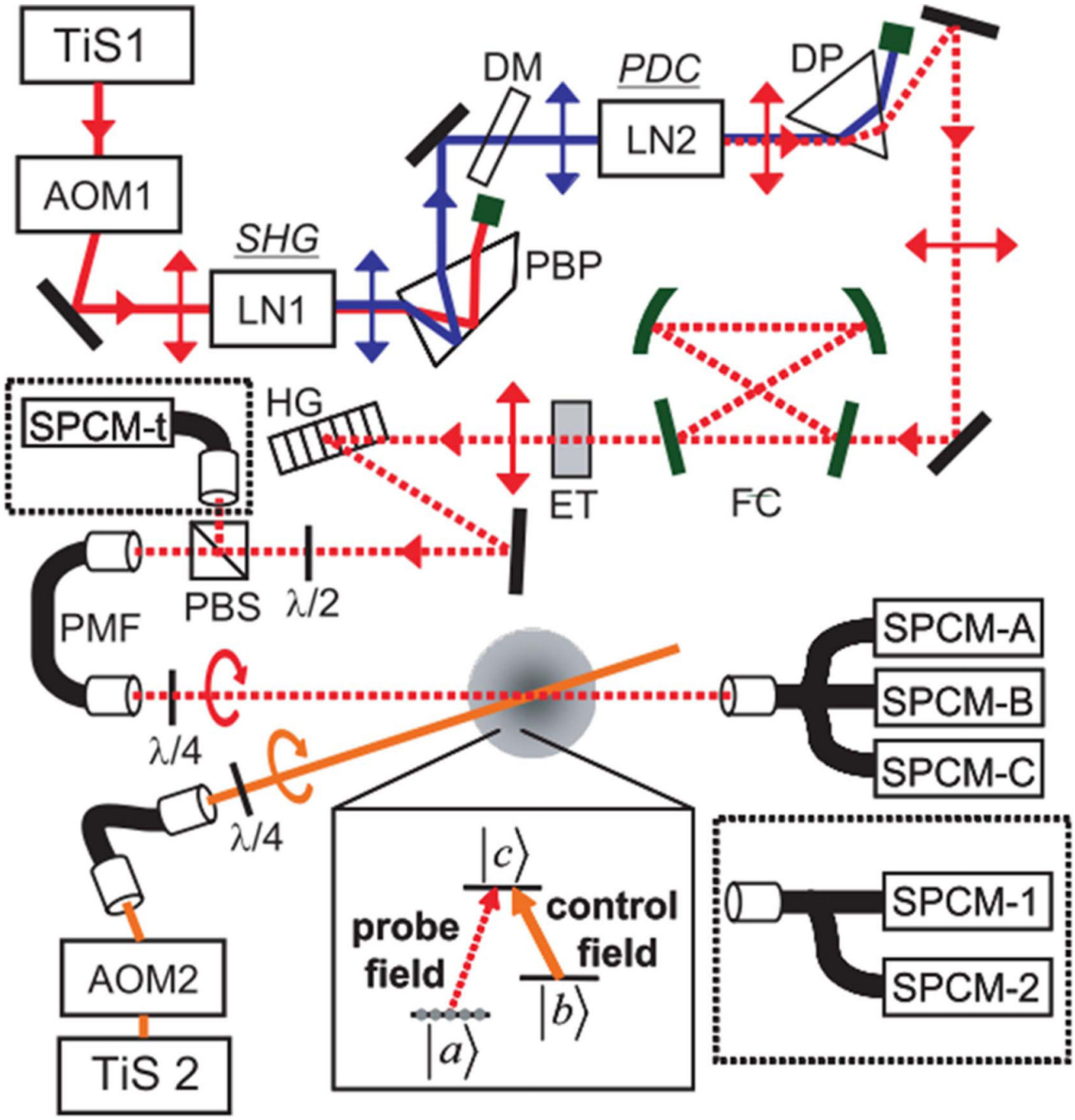

Figure 12.

Storage and retrieval in EIT quantum memory of nonclassical photon pairs from SPDC. TiS : Ti:sapphire laser; AOM: acousto-optic modulator; LN: quasi-phase-matched $MgO:LiNbO_3$ waveguide; PBP: Pellin–Broca prism; DM: dichroic mirror; DP: dispersing prism; FC: filtering cavity; ET: etalon; HG: holographic grating; $\lambda/2$, $\lambda/4$: half and quarter wave plates; PBS: polarizing beam splitter; PMF: polarization maintaining single-mode fiber; SPCM: single photon counting module. The arrows indicate the polarization of light. Reproduced from [31].

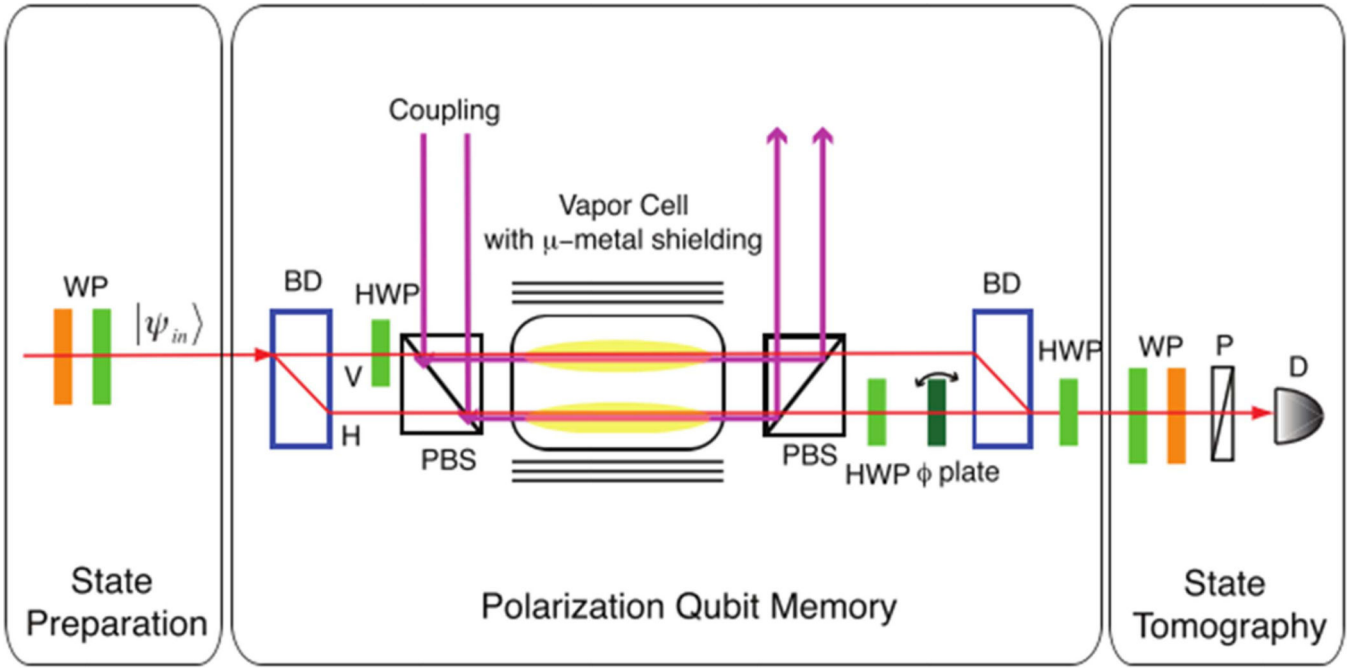

Figure 13.

EIT quantum memory for polarization qubit. WP: wave plate; P: polarizer; BD: beam displacer; HWP: half-wave plate; D: single-photon detector. Reprinted figure with permission from [21], copyright 2016 by The Optical Society.

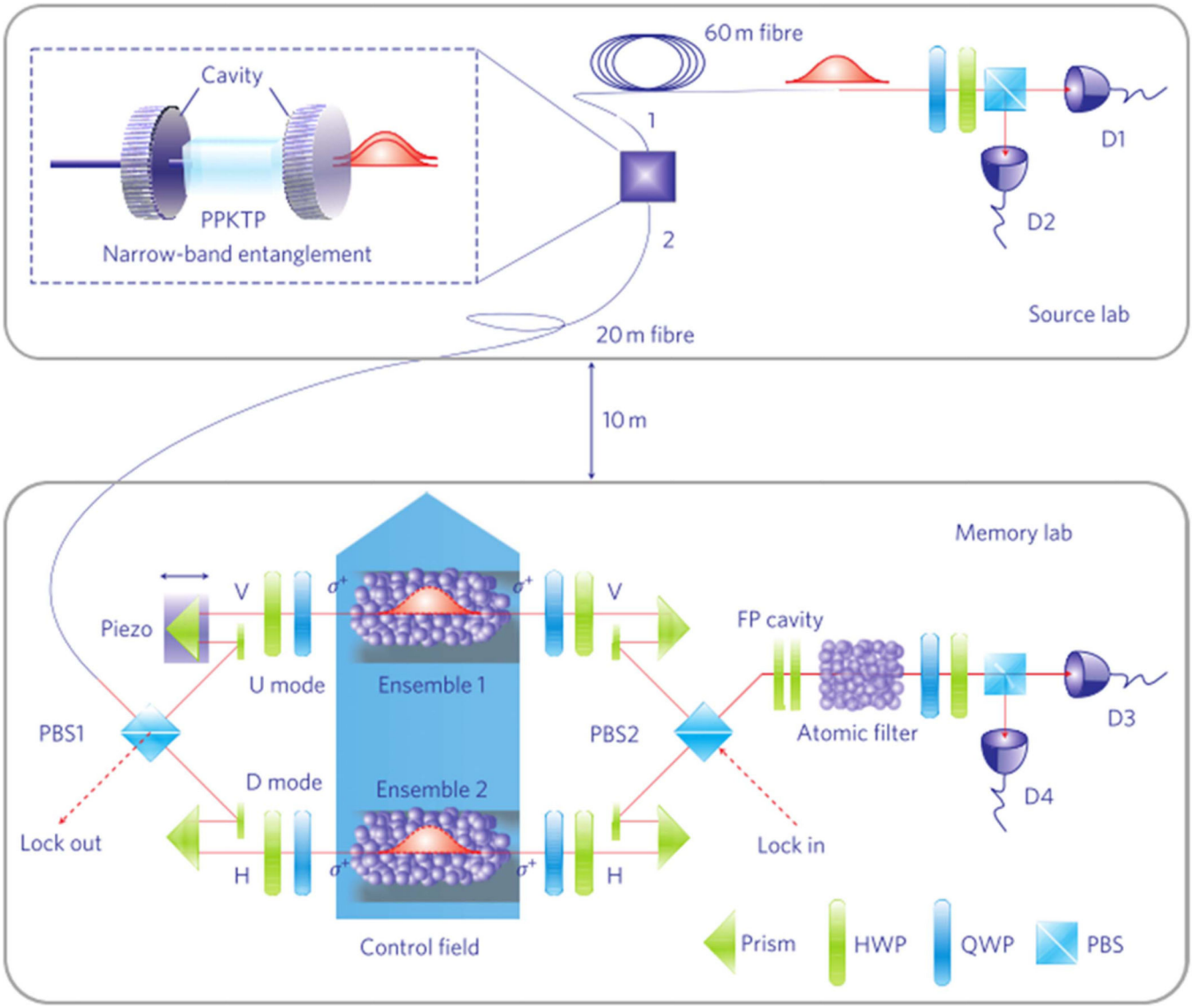

Figure 14.

Preparation and storage of frequency-uncorrelated entangled photons from cavity-enhanced SPDC. Reprinted by permission from Macmillan Publishers Ltd: Nature Photonics [26], copyright (2016).

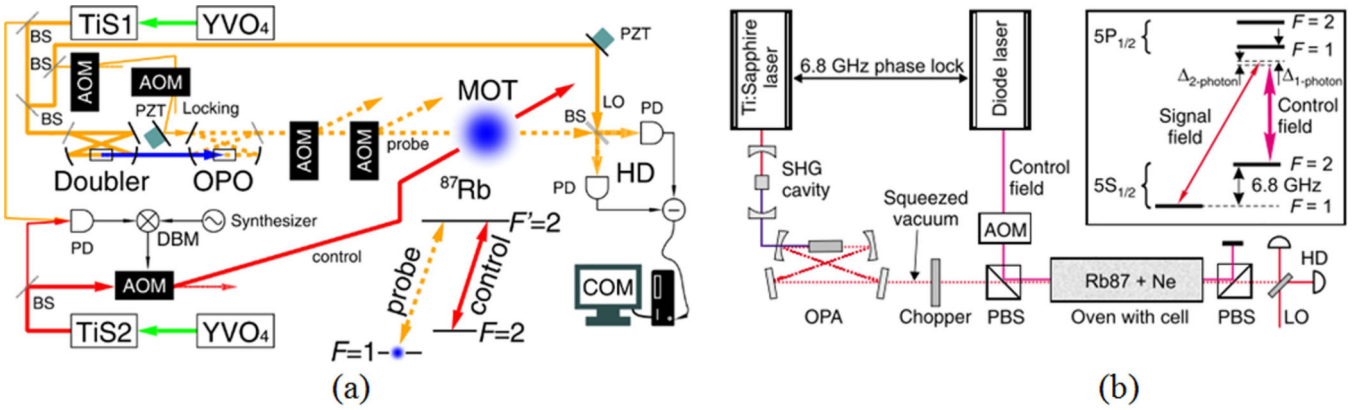

Figure 15.

EIT quantum memory for squeezed vacuum storage. (a) Experiment based on laser trapped Rb atomic ensembles by Kozuma's group. YVO_4: frequency-doubled YVO_4 laser; TiS: Ti:sapphire laser; BS: beam splitter; PD: photo detector; LO: local oscillator; HD: homodyne detector; DBM: double balanced mixer; AOM: acoustic-optical modulator; COM: computer for data acquisition and analysis. Reprinted figure with permission from [146], copyright 2016 by the American Physical Society. (b) Experiment based on warm Rb atomic ensemble by Lvovsky's group. SHG, second harmonic generation; PBS, polarizing beam splitter; LO, local oscillator; HD, homodyne detector; AOM, acousto-optical modulator. Reprinted figure with permission from [22], copyright 2016 by the American Physical Society.

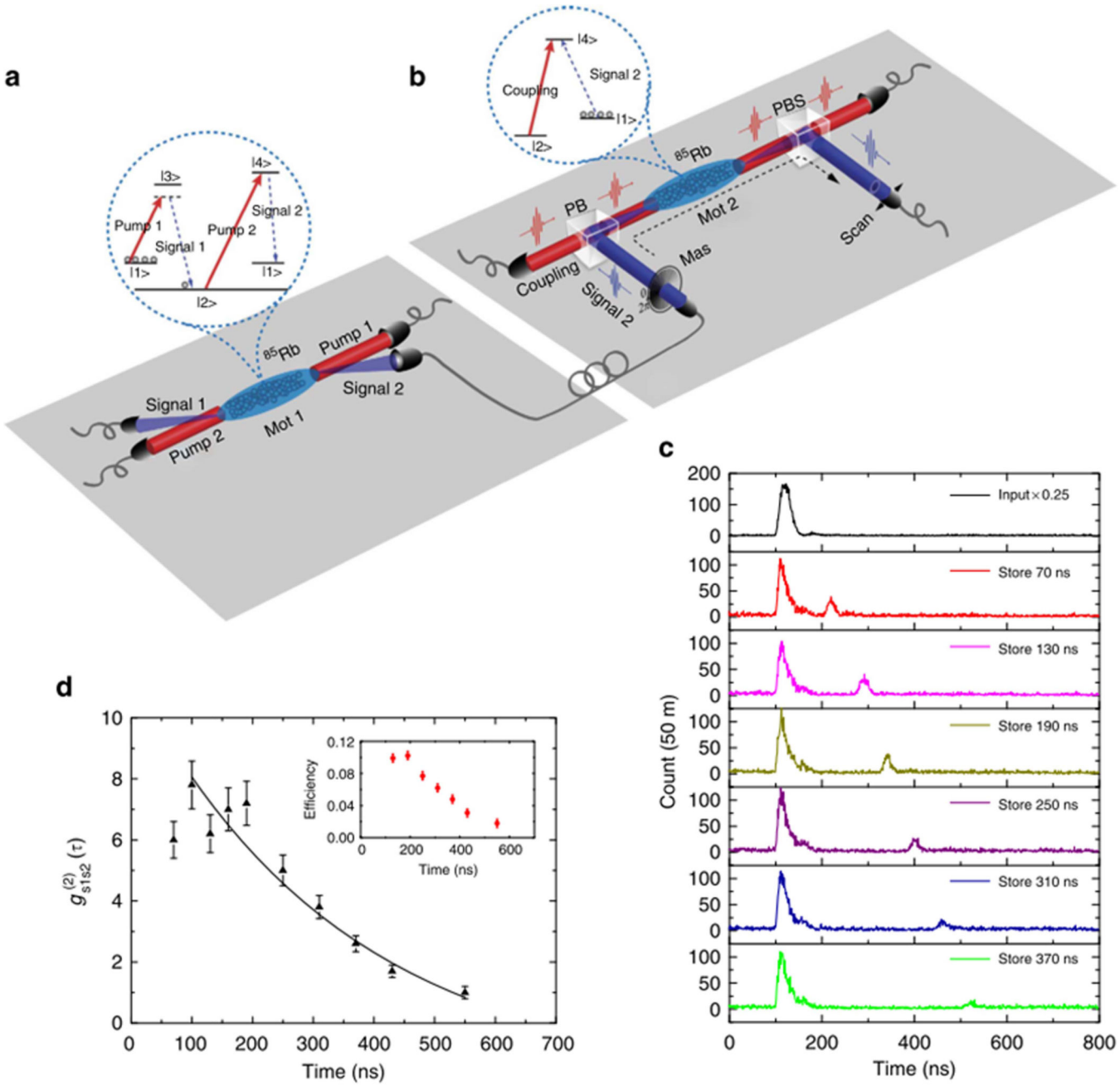

Figure 16.

EIT quantum memory for orbital angular momentum qubit. (a) Generation of non-classical photon correlations using SFWM, (b) EIT memory for photons (c) coincidence counts between the retrieved signal and the trigger as a function of storage time. (d) Cross-correlation function between the retrieved signal and the trigger photons. Reprinted by permission from Macmillan Publishers Ltd: Nature Communications [157], copyright (2016).

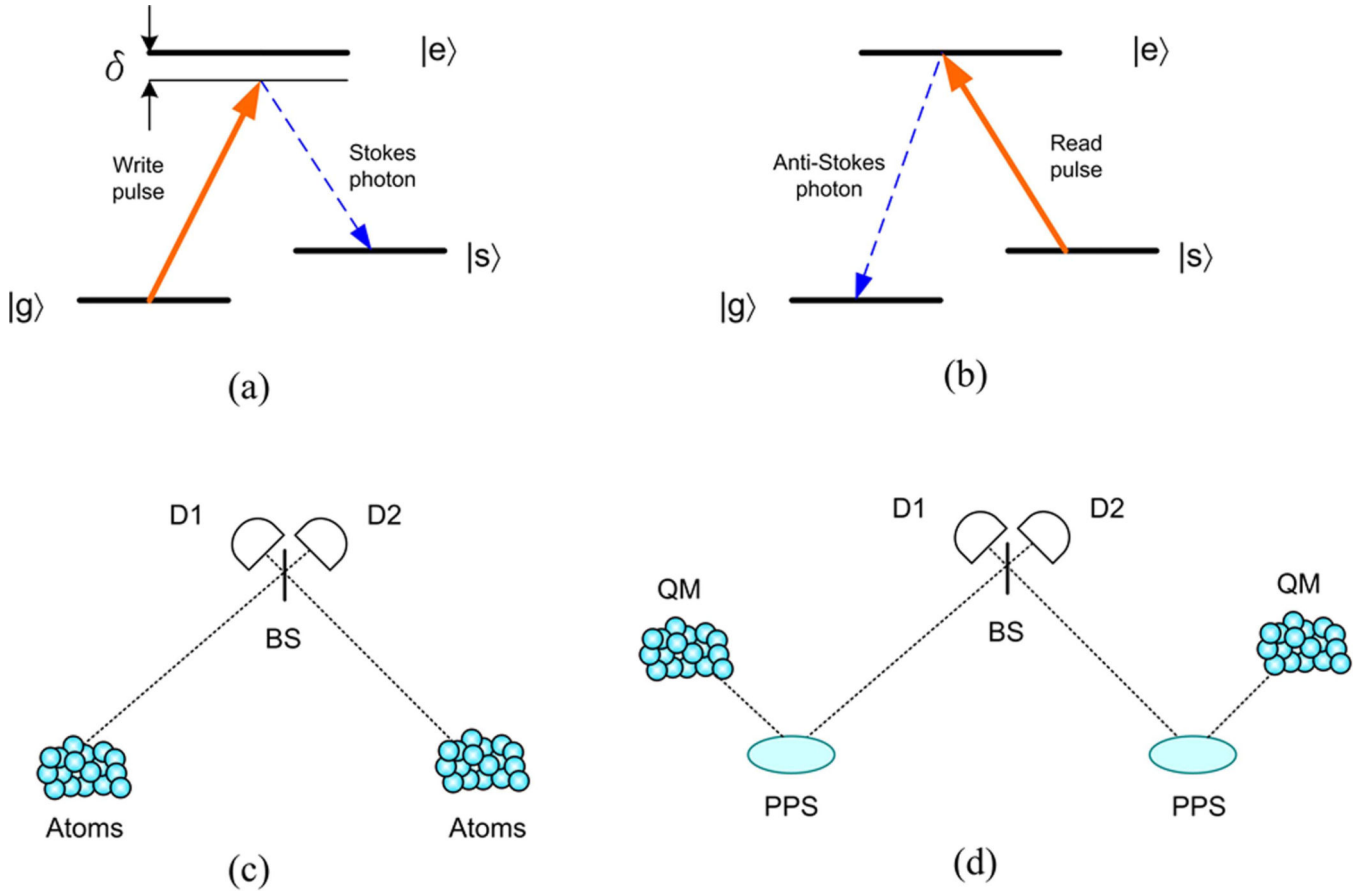

Figure 17.

The DLCZ protocol. (a) and (b) The write and read process in DLCZ; (c) entanglement generation of two atomic ensembles in DLCZ protocol. (d) An approach with photon pair source and quantum memory to create long-distance entanglement. D1 and D2: detector; QM: quantum memory; PPS: photon pair source, BS: beamsplitter.

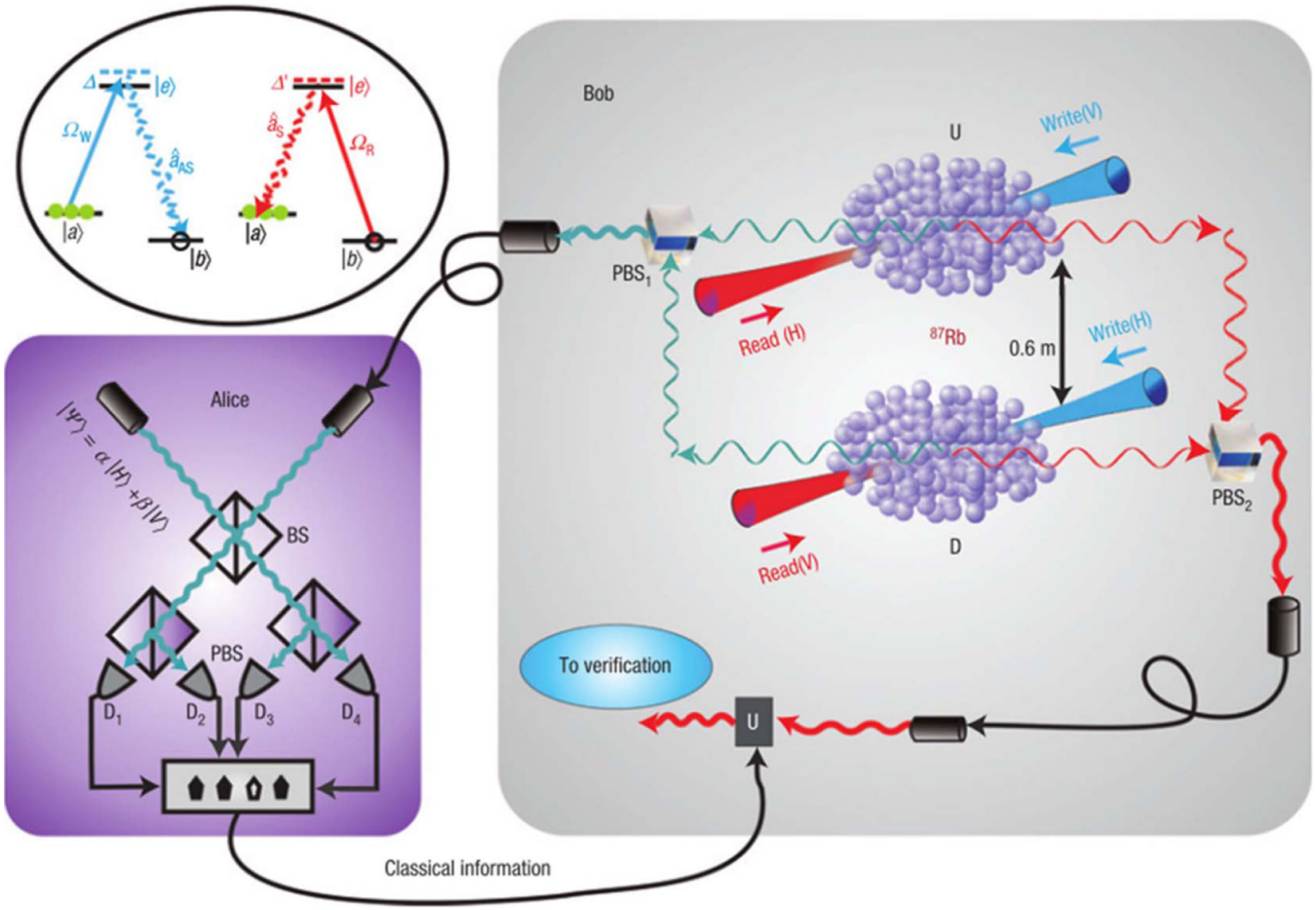

Figure 18.

Memory-built-in quantum teleportation with photonic and atomic qubits. Reprinted by permission from Macmillan Publishers Ltd: Nature Physics [28], copyright (2016).

Table 1

Overview of main approaches to quantum memories.

Category	Approach	Readout	Main storage media[a]	Bandwidth[b] (MHz)	Efficiency[c] (%)	Storage time[d] (ms)	Noise	Multimode capacity
Optically controlled	EIT	On demand	Cold or warm gas, solid state	0.1–10^2	78 [72]	10^3 [37]	Moderate	Low
	Raman	On-demand	Cold or warm gas, solid state	10^2–10^6	30 [44]	1.5×10^{-3} [40]	High	Low
Engineered absorption	CRIB/GEM	Pre-determined	RE-doped solid state, warm gas	10–10^3	80 [76]	0.2 [76]	Low	Moderate
	AFC	Pre-determined	RE-doped solid state	10–10^3	56 [77]	5×10^{-3} [78]	Low	High
Hybrid	Raman-GEM	On-demand with delay	warm gas	10–10^3	87 [59, 62]	1[62]	Low	Moderate
	Λ-AFC	On-demand with delay	RE-doped solid state	10–10^3	12 [63]	1[64]	Low	High

[a] An approach could be implemented in a variety of storage media. The table only lists the most popular media that is used for the corresponding approach.

[b] The bandwidth is not only dependent on the approach, but also on the storage media and other factors. The table lists a range of bandwidth of quantum memories based on the corresponding approach.

[c] The efficiency refers to the highest that has been demonstrated so far.

[d] The storage time refers to the longest that has been demonstrated so far.